

WESTINGHOUSE RESEARCH AND DEVELOPMENT CENTER PITTSBU--ETC F/G 20/2  
RIBBON GROWTH OF SINGLE CRYSTAL GAAS FOR SOLAR CELL APPLICATION--ETC(U)  
NOV 81 T A GOULD, R G SEIDENSTICKER F33615-78-C-2031  
81-9F4-GARSH-R1 AFWAL-TR-81-2115 NL

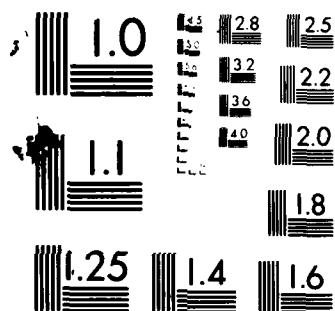
UNCLASSIFIED

AFWAL-TR-81-2115

NL

1. 1. 1.

END  
DATE  
FILMED  
4 82  
DTIC



MICROCOPY RESOLUTION TEST CHART  
NATIONAL BUREAU OF STANDARDS 1963-A

ADA112038

AFWAL-TR-81-2115

RIBBON GROWTH OF SINGLE CRYSTAL  
GaAs FOR SOLAR CELL APPLICATION

Westinghouse R&D Center  
1310 Beulah Road  
Pittsburgh, Pennsylvania 15235

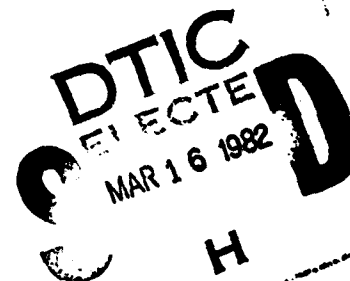
November 1981

Final Report for Period 15 August 1978 - 15 August 1981

Approved for public release; distribution unlimited.

DTIC FILE COPY

AERO PROPULSION LABORATORY  
AIR FORCE WRIGHT AERONAUTICAL LABORATORIES  
AIR FORCE SYSTEMS COMMAND  
WRIGHT-PATTERSON AIR FORCE BASE, OHIO 45433



82 03 16 025

NOTICE

When Government drawings, specifications, or other data are used for any purpose other than in connection with a definitely related Government procurement operation, the United States Government thereby incurs no responsibility nor any obligation whatsoever; and the fact that the government may have formulated, furnished, or in any way supplied the said drawings, specifications, or other data, is not to be regarded by implication or otherwise as in any manner licensing the holder or any other person or corporation, or conveying any rights or permission to manufacture use, or sell any patented invention that may in any way be related thereto.


This report has been reviewed by the Office of Public Affairs (ASD/PA) and is releaseable to the National Technical Information Service (NTIS). At NTIS, it will be available to the general public, including foreign nations.

This technical report has been reviewed and is approved for publication.

  
W. PATRICK RAHILLY  
Project Engineer

  
JOSEPH W. WISE  
TAM, Solar/Thermal

FOR THE COMMANDER

  
JAMES D. REAMS  
Chief, Aerospace Power Division  
Aero Propulsion Laboratory

"If your address has changed, if you wish to be removed from our mailing list, or if the addressee is no longer employed by your organization please notify \_\_\_\_\_, W-PAFB, OH 45433 to help us maintain a current mailing list".

Copies of this report should not be returned unless return is required by security considerations, contractual obligations, or notice on a specific document.

Unclassified

SECURITY CLASSIFICATION OF THIS PAGE (When Data Entered)

REPORT DOCUMENTATION PAGE		READ INSTRUCTIONS BEFORE COMPLETING FORM
1. REPORT NUMBER AFWAL-TR-81-2115	2. GOVT ACCESSION NO. <b>AD-A112 038</b>	3. RECIPIENT'S CATALOG NUMBER
4. TITLE (and Subtitle) RIBBON GROWTH OF SINGLE-CRYSTAL GaAs FOR SOLAR CELL APPLICATION		5. TYPE OF REPORT & PERIOD COVERED Final Report Aug. 15, 1978-Aug. 15, 1981
		6. PERFORMING ORG. REPORT NUMBER 81-9F4-GARSH-R1
7. AUTHOR(s) Theresa A. Gould, Raymond G. Seidensticker, and Robert Mazelsky		8. CONTRACT OR GRANT NUMBER(s) Air Force Contract F33615-78-C-2031
9. PERFORMING ORGANIZATION NAME AND ADDRESS Westinghouse Electric Corporation 1310 Beulah Road Pittsburgh, PA 15235		10. PROGRAM ELEMENT, PROJECT, TASK AREA & WORK UNIT NUMBERS 62203F 31451968
11. CONTROLLING OFFICE NAME AND ADDRESS Aero Propulsion Laboratory (AFWAL/POOC-2) Air Force Wright Aeronautical Laboratories (AFSC) Wright-Patterson Air Force Base, Ohio 45433		12. REPORT DATE November 1981
		13. NUMBER OF PAGES 66
14. MONITORING AGENCY NAME & ADDRESS (if different from Controlling Office) DCASMA-Pittsburgh 1610-S. Federal Building 1000 Liberty Avenue Pittsburgh, PA 15222		15. SECURITY CLASS. (of this report) Unclassified
15a. DECLASSIFICATION/DOWNGRADING SCHEDULE		
16. DISTRIBUTION STATEMENT (of this Report)  Approved for public release; distribution unlimited.		
17. DISTRIBUTION STATEMENT (of the abstract entered in Block 20, if different from Report)		
18. SUPPLEMENTARY NOTES		
19. KEY WORDS (Continue on reverse side if necessary and identify by block number)  gallium arsenide, ribbon, web, dendrites, encapsulation, modelling, growth, solar, cells, twins, faceting, doping, undercooling, morphology.		
20. ABSTRACT (Continue on reverse side if necessary and identify by block number)  This report describes the results of a 3-year effort to develop GaAs dendritic web for high-efficiency solar cells. A unique GaAs ribbon growth system was developed by applying dendritic-web growth techniques to a liquid-encapsulated GaAs system. Computerized thermal modelling and experimental modification produced a thermal geometry from which 48 GaAs webs were grown. These crystals had a multidendrite and/or faceted morphology rather than typical web morphology. Crystal quality improved as thermal geometry,		

DD FORM 1 JAN 73 1473 EDITION OF 1 NOV 65 IS OBSOLETE

Unclassified

SECURITY CLASSIFICATION OF THIS PAGE (When Data Entered)

cont ii

20. Abstract (Cont.)

growth techniques, dendrite seeds, and melt chemistry were optimized during the course of the program; however, conventional web morphology was not achieved. Analyses of chemical modification, crystal-growth characteristics, and orientation relationships suggest that inherent materials properties of GaAs produce an atypical web morphology under conventional web-growth conditions. Consequently, a simple transfer of Si web growth technology to our GaAs system was inadequate for the growth of high quality GaAs web. We believe that typical web morphology of GaAs and other polar compounds will be achieved only if sophisticated, fundamental studies determine specialized chemical and/or thermal conditions which will support conventional web growth of these materials.

**BLANK PAGE**

# FOREWORD

This Technical Report covers all work performed under Contract No. F33615-78-C-2031, entitled "Ribbon Growth of Single-Crystal GaAs for Solar Cell Application." The effort was sponsored by the Aero Propulsion Laboratory, Air Force Systems Command, Wright-Patterson Air Force Base, Ohio under Project 3145. Dr. W. Patrick Rahilly (AFWAL/POOC-2) was the Air Force Project Engineer, while Theresa Gould of Westinghouse Electric Corporation was technically responsible for the work.

The authors wish to thank A. M. Stewart for his capable technical assistance throughout the program. The construction of the thermal model by E. Miksch is also acknowledged. Appreciation is extended to D. L. Barrett, C. S. Duncan, R. H. Hopkins, J. P. McHugh, and T. J. Isaacs for many helpful discussions, and to T. J. Mullen, A. Koranovich, P. G. McMullin, and R. C. Clarke for their assistance with the characterization work.

Accession For	
NTIS GRA&I	<input checked="" type="checkbox"/>
DTIC TAB	<input type="checkbox"/>
Unannounced	<input type="checkbox"/>
Justification	
By _____	
Distribution/	
Availability Codes	
Dist	Avail and/or Special
A	



## TABLE OF CONTENTS

SECTION	PAGE
I. INTRODUCTION . . . . .	1
II. EXPERIMENTAL METHODS . . . . .	4
2.1 Growth Facility . . . . .	4
2.2 Materials . . . . .	7
2.3 Crystal Growth and Characterization Procedures. . . . .	7
III. WEB GROWTH RESULTS . . . . .	12
3.1 Results Synopsis. . . . .	12
3.2 Thermal Geometry. . . . .	19
3.2.1 Thermal Modelling. . . . .	19
3.2.2 Ge Thermal Analog. . . . .	21
3.2.3 Empirical Thermal Modification and Evaluation. . . . .	25
3.3 Seeds . . . . .	27
3.4 Doping Effects. . . . .	32
IV. CHARACTERIZATION . . . . .	37
4.1 General Description . . . . .	37
4.2 Twin Structure. . . . .	39
4.3 Composition . . . . .	43
4.4 Dislocations. . . . .	45
4.5 Electrical Properties and Impurities. . . . .	45
V. ORIENTATION ANALYSIS . . . . .	48
VI. CONCLUSIONS. . . . .	57
VII. SUMMARY. . . . .	64
REFERENCES . . . . .	65

PRECEDING PAGE BLANK-NOT READ



## LIST OF ILLUSTRATIONS

FIGURE		PAGE
1	Schematic Section of Web Growth	3
2	The Modified A. D. Little Furnace Used During Phase II. The Afterchamber Provided Access to Crystals and Seeds While Temperature and Pressure in the Main Chamber Remained Undisturbed.	5
3	Web-Growth Susceptor Assembly. The Design of Susceptor #1 in which a Small Gap was Left Under the Crucible is Indicated by the Dashed Line. The Design of Susceptor #2 which Fits the Spherical Portion of the Crucible Smoothly is Indicated by the Full Line.	6
4A	"Dogbone" Slot Shape and Dimensions of Lid #4 Used for the Majority of the Phase II Growth Experiments.	8
4B	The Standard Growth Configuration which Incorporated Lid #4 and Shields of the Given Thicknesses.	8
5	Cross Section of an Odd-Twin-Plane Dendrite Etched with $\text{HNO}_3:\text{H}_2\text{O};4:3$ . The $[211]$ Direction at the Top of the Crystal Responded to the Etch Faster than the $[2\bar{1}\bar{1}]$ Section at the Bottom.	10
6	First Piece of Multidendrite Web Grown From the Liquid-Encapsulated System.	13
7	Long Multidendrite Web Grown From First Test of the Modified Furnace.	14
8	Multidendrite Crystal Having Flat, Faceted Areas. These Crystals Grew when Thin Radiation Shields Were Incorporated into the Thermal Configuration.	15
9	Segment of Te-Doped Crystal Exhibiting Strongly Faceted Web.	16
10	Crystal Grown From a Melt Doped With 1.0 Atomic% Ge. The Ge-Doped Crystals Grew at Low Undercooling and Contained Flatter Textured-Web Areas and Fewer Dendrites than Typical Undoped or Te-Doped Crystals.	17

# LIST OF ILLUSTRATIONS (Cont.)

FIGURE		PAGE
11	Short Crystal Grown with 0.5 Atomic% Ge Melt Doping. The Textured-Web Sections Were the Widest Achieved at Small Undercooling, $<5.0^{\circ}\text{C}$ .	18
12	Radiation Exchange Between the Melt Surface and the Lid. The Conventional Radiation Exchange (upper figure) was Altered by Refraction in the $\text{B}_2\text{O}_3$ (lower figure).	20
13	Vertical Thermal Profile for Model Incorporating Susceptor #2. The Profile is a Vertical Cross Section Through the Melt From the Center to the Right Edge, Parallel to the Long Axis of the Slot. Inversion of the Isotherms Occurs at the $\text{GaAs-B}_2\text{O}_3$ Interface.	22
14	Ge Web Grown from Our System to Test the Viability of the Thermal Geometry for Web Growth.	24
15	Morphology Comparison of a Crystal Grown with Radiation Shielding (Left) to One Grown Without Radiation Shielding (Right). The Flat, Faceted Areas Resulted From the Improved Thermal Geometry.	26
16	"Artificial" Twin Plane (indicated by the arrow) Generated by the "Double Seed" Experiment. Other Twin Structures Visible Were Nucleated From the Two Halves of the Double Seed.	30
17	Comparison of Three Ge-Doped Crystals (left) to an Undoped Button (right). The Faceted Morphology was Improved and Branching Growth was Reduced in the Narrow Ge-Doped Crystals.	33
18	Close-up of Ge-Doped Textured Web which was Composed of Small Facets.	34
19	Comparison of a Typical Crystal Surface Marked by Ga Droplets Running in the Growth Direction (upper photo) With Surface of a Crystal Grown With 3.0 Atomic% Ge Melt Doping (lower photo).	35
20	Optical Micrograph of Surface Facet Orientation. The Triangular Etch Pits which Point the $[2\bar{1}\bar{1}]$ Direction Remained Aligned Across Facet Boundaries.	40
21	SEM Micrographs of Surface Facets on a Ge-Doped Crystal. In Some Areas Flow Boundaries Formed Regular Patterns (upper photo). In Other Areas the Facets Were Bounded By Crystallographic Planes (lower photo).	41

# LIST OF ILLUSTRATIONS (Cont.)

FIGURE		PAGE
22	SEM Photo of Droplet Formation Yielding Depressions Bounded by (111) Planes. The Droplets were Pure Ga, but the Trails and Depressions and the Smooth Regions (area 1) were Stoichiometric GaAs.	44
23	Typical Dislocation Density and Distribution in GaAs Dendrite and Web Samples.	46
24	Orientation Analysis of GaAs Web Assuming a Faceted Interface. The $[2\bar{1}\bar{1}]$ Growth Direction is Bounded by an As $[1\bar{1}\bar{1}]$ Plane While the $[\bar{2}11]$ Growth Direction is Bounded by a Ga $[\bar{1}11]$ Plane.	49
25	SEM Photo of Etched Four-Twin-Plane Cross Section. The Raised Steps are the $[2\bar{1}\bar{1}]$ Twinned Sections which were More Etch Resistant Than the $[\bar{2}11]$ Crystal. Each Twin was Bounded by One Vertical Step (light line) and One Shallow Step (dark band) which Delineate the Closest $\{111\}$ As Planes (see Figure 26).	50
26	Schematic Section of $\text{HNO}_3$ Etchant Effect Illustrating the As Planes which Form the Twin Boundaries. Compare the Right-Hand Section to Figure 25.	51
27A-C	Morphology Comparison of Ga and As Faces of $[2\bar{1}\bar{1}]$ and $[\bar{2}11]$ Dendrites; Growth Direction to the Left. A) $[2\bar{1}\bar{1}]$ , Ga Face; B) $[2\bar{1}\bar{1}]$ , As Face; C) $[\bar{2}11]$ , As Face.	53
27D,E	D) $[\bar{2}11]$ , Ga Face, E) Equilibrium Form of GaAs Crystal Bounded by both Ga and As $\{111\}$ Planes (Adapted from Ref. 18).	54
28	Possible Three-Twin-Plane Interface Types. For Si Web, Only the Web Interface is Observed. The Inverted Interface Predominated in Our GaAs Crystals.	55
29	The Influence of Thermal and Doping Changes on the Undercooling Required for Growth. (Data Show the Undercooling Range Experienced By a Crystal During Growth, Not Error Bars.) Thermal Modifications Reduced the Undercooling but "Warmer" Lids and Shields Caused Seed Damage. Conventional Undercooling Values Were Achieved Only With Ge Doping.	58
30	Twin-Structure Breakdown in a Three-Twin-Plane GaAs Button Polished Vertically From the Seed to a Depth of 1.3cm. Twin Planes Developing Incoherent Loops Above Were Lost From the Crystal in Subsequent Sections.	59

# LIST OF ILLUSTRATIONS (CONCLUDED)

FIGURE		Page
31	Schematic Section of Web Growth Illustrating the Faceted Interface. Layer Spreading is Initiated by Corner Nucleation at the Intersection of the Dendrite and the Web.	61
32	{111} Faceting in Untwinned and Twinned Diamond or Zinc Blende Solids. A) Equilibrium Form of the Untwinned Solid; B) Ridge and Reentrant Corner Structure Produced by Two Twin Planes; C&D) Nucleation at Type I Reentrant Corners Produces Type II Corners Generating an Indestructable System of Reentrancies By which Twinned Dendrites Propagate. (Adapted From Ref. 23).	62

# LIST OF TABLES

TABLE		PAGE
1	Comparison of Thermal Probing and Modelling Results. . . .	28
2	Vertical Twin-Plane Continuity . . . . .	31
3	Crystal Dimensions . . . . .	38
4	Twin-Spacing Summary . . . . .	42

## SECTION I

### INTRODUCTION

This report describes the results of a three-year effort, from August 1978 through August 1981, to develop gallium arsenide dendritic web for high-efficiency solar cells. The results of the first twelve months of the program (Phase I) were reviewed and evaluated before the remainder of the program (Phase II) was undertaken. An interim report<sup>(1)</sup> describes the work performed during Phase I, and therefore those results are discussed only briefly in this final report.

The overall goal of the program was to demonstrate the utility of the dendritic-web process for economical production of solar cell base material. Significant progress toward this goal was achieved; however, high-quality GaAs web crystals of conventional web morphology were not obtained apparently due to fundamental crystal-growth properties of the GaAs.

The major thrust of Phase I was to assess the feasibility of growing GaAs dendritic web from a liquid-encapsulated system. Crystal growth and thermal modelling were performed concurrently. Twinned dendrites and buttons--which are precursors of web growth--were obtained, and the modelling results indicated that the thermal conditions required for dendritic-web growth could be achieved.

During Phase II, a significant adjustment in thermal geometry suggested by the modelling resulted in the growth of primitive ribbon crystals. Subsequently, the growth system was modified to produce greater flexibility, and the efficiency of the experimental work increased. Further improvements in thermal geometry, growth techniques, seed quality, and melt chemistry produced some improvements in material morphology and reproduction of results. However, crystal quality appeared to be ultimately limited by the atomic attachment kinetics and the polar nature of the GaAs itself.

The dendritic-web technique is illustrated schematically in Figure 1. A seed dendrite with the required twin-plane structure is brought into contact with the melt at the "hold" temperature. At this temperature the seed neither melts nor nucleates growth. As the melt is undercooled, the twin structure of the seed and the attachment kinetics associated with the thermal environment induce the growth of a lateral "button." When the button is pulled from the melt, two dendrites propagate from the ends and a film of liquid is drawn up between them. This film freezes into a single-crystal ribbon the smooth surface of which is well suited for subsequent device fabrication.<sup>(2)</sup>

The dendritic-web process has been highly successful for growth of single-crystal silicon ribbons.<sup>(3)</sup> Dendritic morphology in GaAs was demonstrated in 1964.<sup>(4)</sup> However, good-quality dendritic web was not obtained due to inadequate control of arsenic vaporization from the melt. Also, the prior experiments were impeded by insufficient optimization of the thermal conditions in the growth system.

Two technologies have been developed that overcome the shortcomings of these initial experiments. The first is the liquid-encapsulation technique, which provides a simple method to control dissociation of volatile compounds.<sup>(5)</sup> Liquid encapsulation with boric oxide has become widely used for Czochralski growth of GaAs<sup>(6-11)</sup> and was adopted for the current web-growth experiments.

A second major advance in web-growth technology is the systematic optimization of growth conditions by thermal modelling. An existing computerized heat-flow analysis, which had been developed for silicon systems,<sup>(12)</sup> was adapted for use with the liquid-encapsulated GaAs system.

Dwg. 7721A17

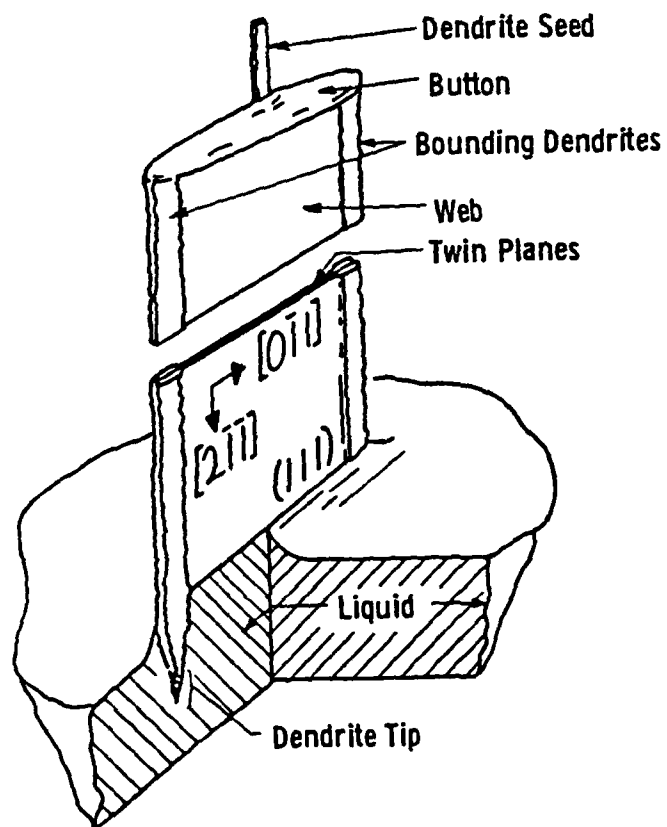


Figure 1 Schematic Section of Web Growth



## SECTION II

### EXPERIMENTAL METHODS

#### 2.1 Growth Facility

An A. D. Little furnace, which was heated by induction with a molybdenum susceptor, was used for the crystal-growth experiments. Replacement of the lower pulling unit with a susceptor support assembly provided thermal isolation of the susceptor, thermocouple access, and vertical positioning of the susceptor with respect to the coil.

A subsequent major modification performed during Phase II of the program increased the flexibility and efficiency of the system. The upper pulling unit was replaced by an afterchamber and extended pulling apparatus that were fabricated in-house (Figure 2). The afterchamber provided access for removal of grown material and seed changes without terminating the experiment in progress. During a growth run the unit could be isolated from the main chamber by a ball valve, depressurized, and opened as often as necessary.

The susceptor assembly is shown in Figure 3. An AZAR L&N controller, which responded to the light-pipe output from the outer susceptor wall, maintained temperatures to within  $\pm 0.1^\circ\text{C}$ . Temperatures were measured by a sealed, molybdenum-sheathed, Type B thermocouple in the axial position.

Fused-quartz crucibles two inches in diameter obtained from Amersil and Thermal American were used in the system. In order to minimize heat-transfer variations induced by small differences in crucible fit, a small gap was left below the crucible in susceptor #1 (dashed line, Figure 3). This produced undesirable thermal effects, and susceptor #2 was designed to fit the spherical crucible shape.

The lower radiation shields minimized heat loss from the bottom of the susceptor, and the upper lid and shields imposed the thermal conditions required for web growth on the melt. The lid and shield



Figure 2 The Modified A. D. Little Furnace Used During Phase II. The Afterchamber Provided Access to Crystals and Seeds While Temperature and Pressure in the Main Chamber Remained Undisturbed.

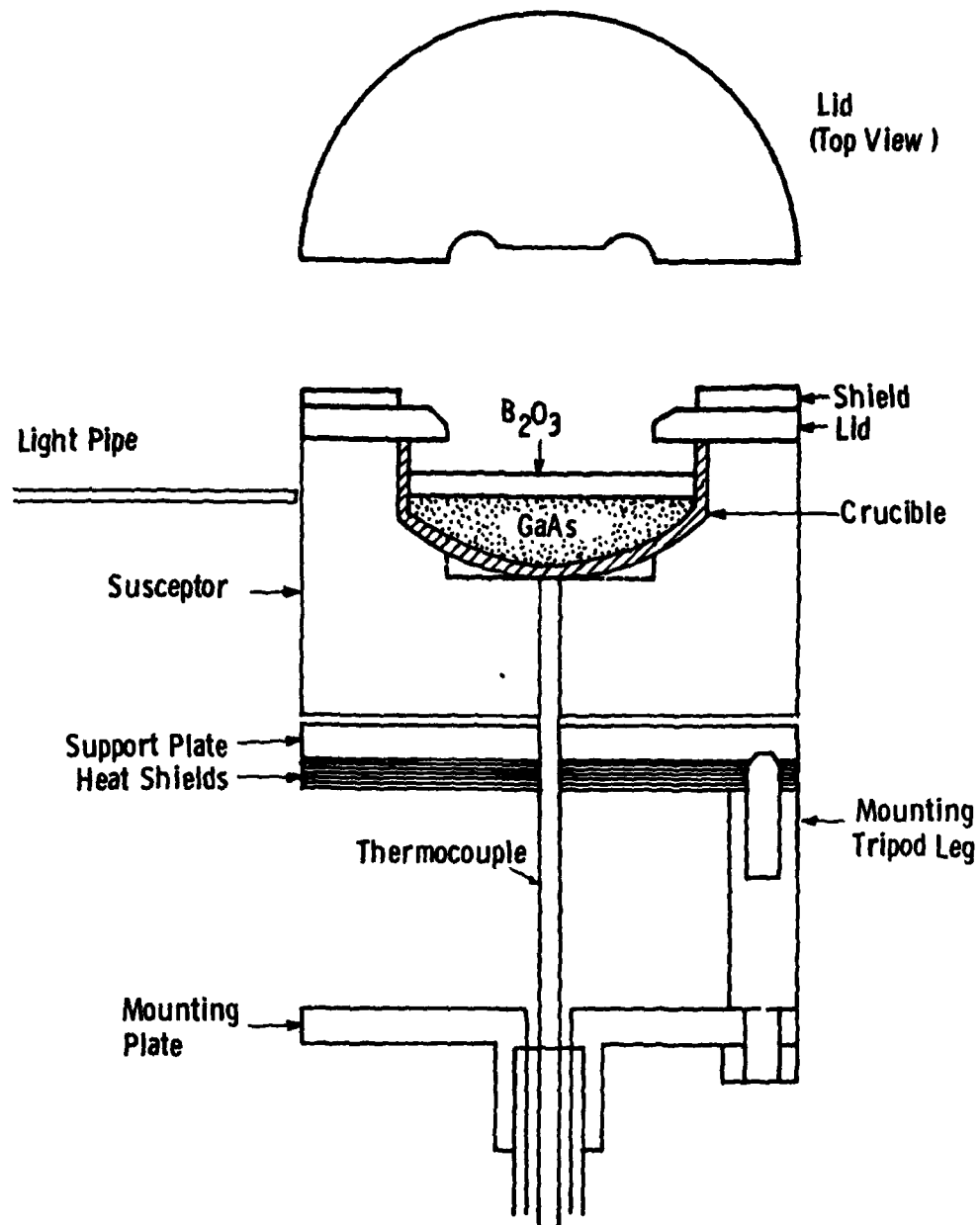


Figure 3 Web-Growth Susceptor Assembly. The Design of Susceptor #1 in which a Small Gap was Left Under the Crucible is Indicated by the Dashed Line. The Design of Susceptor #2 which Fits the Spherical Portion of the Crucible Smoothly is Indicated by the Full Line.

designs shown in Figure 4a&b were used for the majority of the growth experiments in Phase II. The bevelled "dogbone" slot shape was adapted from Si web experience, and we incorporated a 1/4-inch-thick lid with the given slot dimensions in the thermal model and in the early experiments. Subsequently, use of 1) a 1/8-inch-thick lid (lid #4) and 2) thin (0.005 inch) overhanging radiation shields improved the growth behavior and became the typical growth configuration (Figure 4b).

## 2.2 Materials

Semiconductor grade, undoped GaAs (five 9's) obtained from Morgan Semiconductor was used as starting material for much of the experimental work. Single-crystal liquid-encapsulated Czochralski (LEC) GaAs grown from pyrolytic boron nitride crucibles at Westinghouse was also used. No significant differences were observed with variation of starting material.

High-purity  $B_2O_3$  for liquid encapsulation from Atomergic Chemetals Corporation, and Johnson Matthey Puratronic Grade 1  $B_2O_3$  were used for the encapsulant with equal success.

Several different dopants were incorporated in the melt at various stages of the program. ASARCO high-purity, semiconductor-grade tellurium and 40 ohm-cm germanium from Allegheny Electric Corporation were used to dope the GaAs. Five 9's pure lithium fluoride from Harshaw was used to change the wetting behavior of the  $B_2O_3$ .

## 2.3 Crystal Growth and Characterization Procedures

Prior to a growth run, the  $B_2O_3$  was vacuum dried to remove residual water which would produce bubbling and incur As loss from the melt. The  $B_2O_3$  was dried for 14-16 hours at a temperature of  $\sim 1000^\circ\text{C}$  and a vacuum of  $2 \times 10^{-5}$  Torr. It was then cooled in vacuum, removed intact from a 95% platinum-5% gold drying crucible,<sup>(11)</sup> and used immediately to prevent rehydration.

Dwg. 7745A72

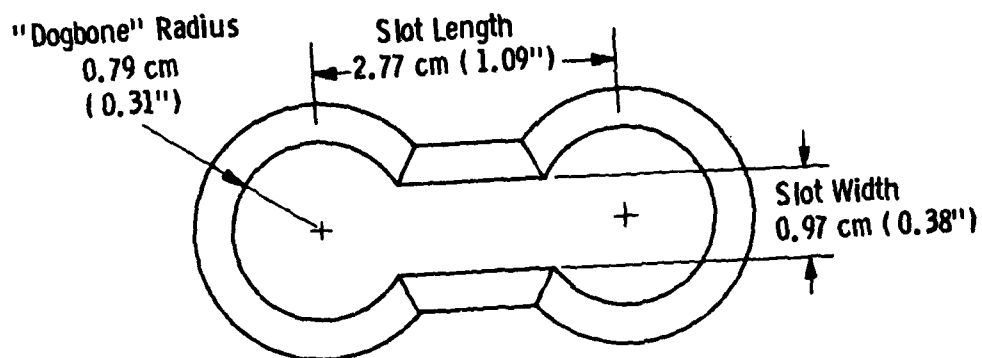


Figure 4A "Dogbone" Slot Shape and Dimensions of Lid #4 Used for the Majority of the Phase II Growth Experiments.

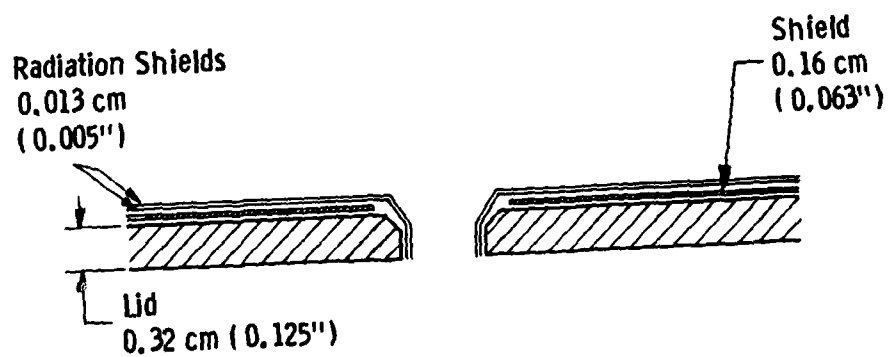


Figure 4B The Standard Growth Configuration which Incorporated Lid #4 and Shields of the Given Thicknesses.

The GaAs seed and charge and the quartz crucible were prepared by etching with aqua regia. Typically, 48-50 grams of GaAs were used with 28-29 grams of  $B_2O_3$ . Use of these masses resulted in a 5- to 6-mm cover layer of  $B_2O_3$  after meltdown.

After the growth configuration was assembled, the furnace was evacuated overnight to  $1-5 \times 10^{-5}$  Torr. The system was pressurized to 30 pounds-per-square-inch gauge with argon prior to heating, yielding a pressure of  $\sim 42$  psig at the growth temperature.

Throughout Phase II, the pull speeds for dendrites and multidendrite webs varied mostly from 1.5-3.0 cm/min. (Faster pulling velocities did not allow time for the  $B_2O_3$  to flow off the crystals, and accumulated  $B_2O_3$  stressed and cracked the GaAs as it solidified.) The undercooling required for stable propagation decreased from 15-25°C at the beginning of Phase II, to 2-5°C at the close of the program.

A Cambridge Stereoscan SEM (Scanning Electron Microscope) was used for microstructural characterization of the as-grown crystal surfaces. Surface chemistry was determined by energy-dispersive spectrometry (EDS) using a Kevex x-ray detector. The standardless EDS analysis yields the elemental composition of the sample to a depth of 1-2  $\mu$  within 3 atomic%.

GaAs dendrites and webs were prepared for twin-structure characterization by potting in Quickmount and polishing. The GaAs was easily chipped and scratched by mechanical polishing but the following sequence of abrasives gave acceptable results: 1) 600-grit wet and dry paper, 2) 3  $\mu$  Microgrit, 3) 1  $\mu$  Linde B, 4) Siton. The twin planes were stained by etching for five to ten seconds with  $HF:H_2O:CrO_3$  (saturated solution), 20:20:1 or by etching for three to five seconds with  $HNO_3:H_2O$ , 4:3. The  $HNO_3$  etch was particularly useful for determining if the number of twin planes was even or odd in samples with a narrow twin structure since the  $[\bar{2}11]$  direction responded to the etch faster than the  $[2\bar{1}\bar{1}]$  direction (Figure 5).

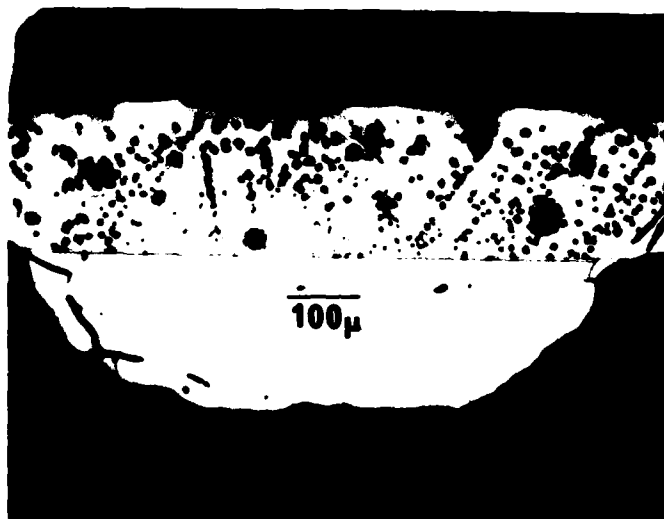


Figure 5 Cross Section of an Odd-Twin-Plane Dendrite Etched with  $\text{HNO}_3:\text{H}_2\text{O};4:3$ . The  $[211]$  Direction at the Top of the Crystal Responded to the Etch Faster Than the  $[211]$  Section at the Bottom.

Surface dislocations were revealed by a four-minute etch in tartaric acid:  $\text{HNO}_3$ , 3:1,<sup>(13)</sup> or by first cleaning the surface with a one- to three-minute AB etch<sup>(14)</sup> and reducing the time in the tartaric-acid etch. (Doped samples were more sensitive to the etchants and required reduced etching times.) Both methods produced triangular etch pits on the gallium face pointing in the  $\langle 2\bar{1}\bar{1} \rangle$  directions.

Web surfaces were prepared for Hall measurements by cleaning with a solution of 50% HCl in propanol. Indium contacts were attached by heating the sample in a hydrogen atmosphere.



## SECTION III

### WEB-GROWTH RESULTS

#### 3.1 Results Synopsis

A total of 48 GaAs crystals were grown during Phase II of the program. In contrast to Si web, which grows as a single, smooth (111) facet bounded by side dendrites (Figure 1), the GaAs webs grew as multidendrite crystals with narrow web areas textured by small, individual (111) facets. Despite their irregular appearance, x-ray and etching results indicated that the GaAs webs were single crystals (neglecting the central coherent twin structure) with the crystallographic orientation of conventional dendritic web shown in Figure 1. Throughout the project, the incorporation of thermal and chemical modifications substantially improved the morphology of our GaAs crystals, as Figures 6-11 illustrate; however, conventional web morphology was not obtained.

The growth behavior and resultant morphology of web crystals are controlled by three basic factors: 1) the thermal geometry of the system (Si-web degenerates to a multidendrite structure if the thermal geometry is incorrect or if the pull speed or undercooling are too great); 2) viable dendrite seeds; and 3) the atomic attachment kinetics of the material.

Our earliest GaAs ribbons were grown at large undercooling and velocities with unconventional seeds. Therefore, the experimental work focussed on reducing the growth parameters into a range more conducive to conventional web growth and improving the quality of our seeds. Adjustment of the thermal geometry produced some improvement in the growth behavior and crystal morphology of both webs and seeds; however, thermal modification was complicated by the effects of the  $B_2O_3$  layer. Chemical alteration of the melt with 0.3-3.0 atomic% Ge produced a substantial



Figure 6 First Piece of Multidendrite Web Grown From the Liquid-Encapsulated System.

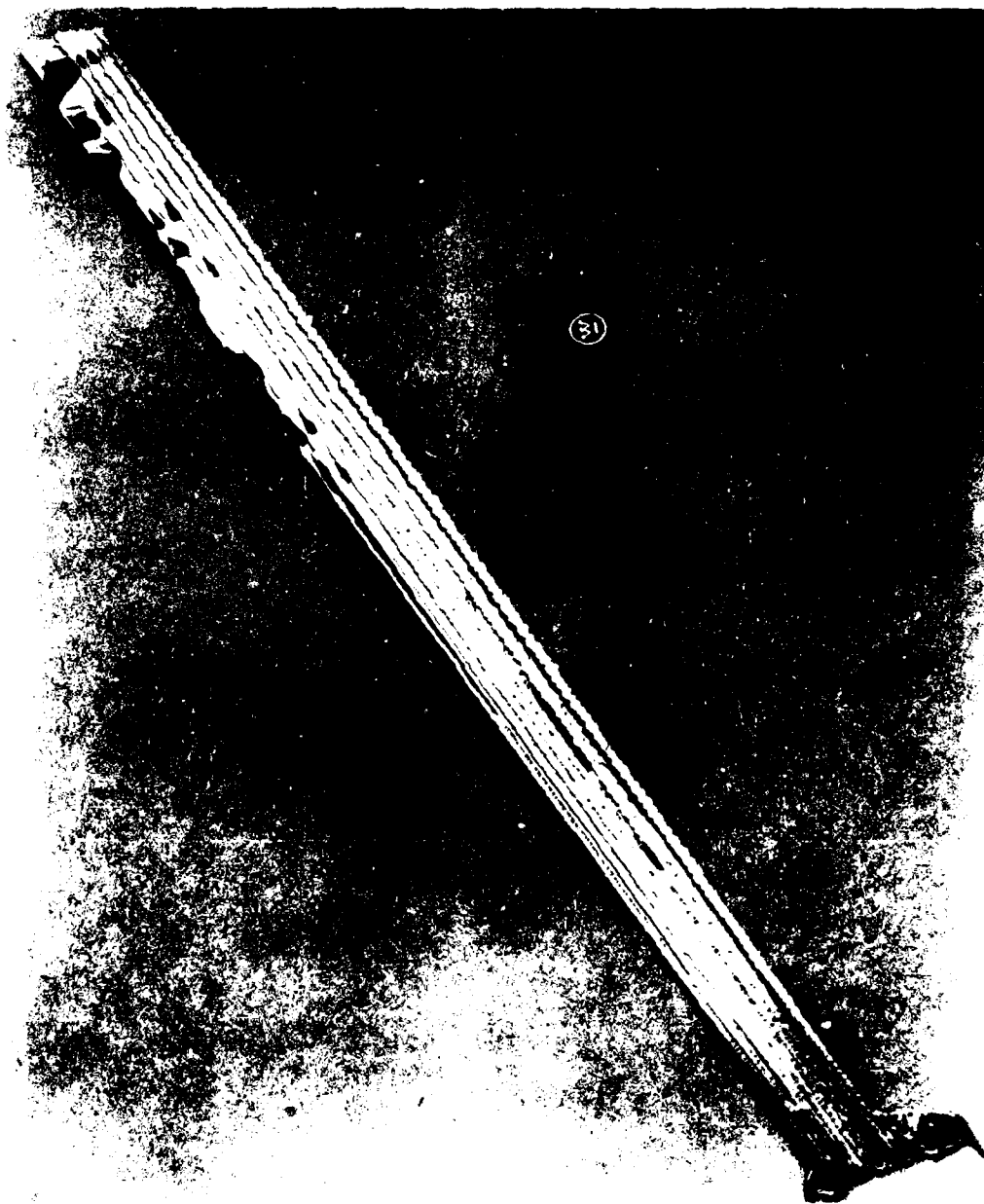


Figure 7 Long Multidendrite Web Grown From First Test of the Modified Furnace.

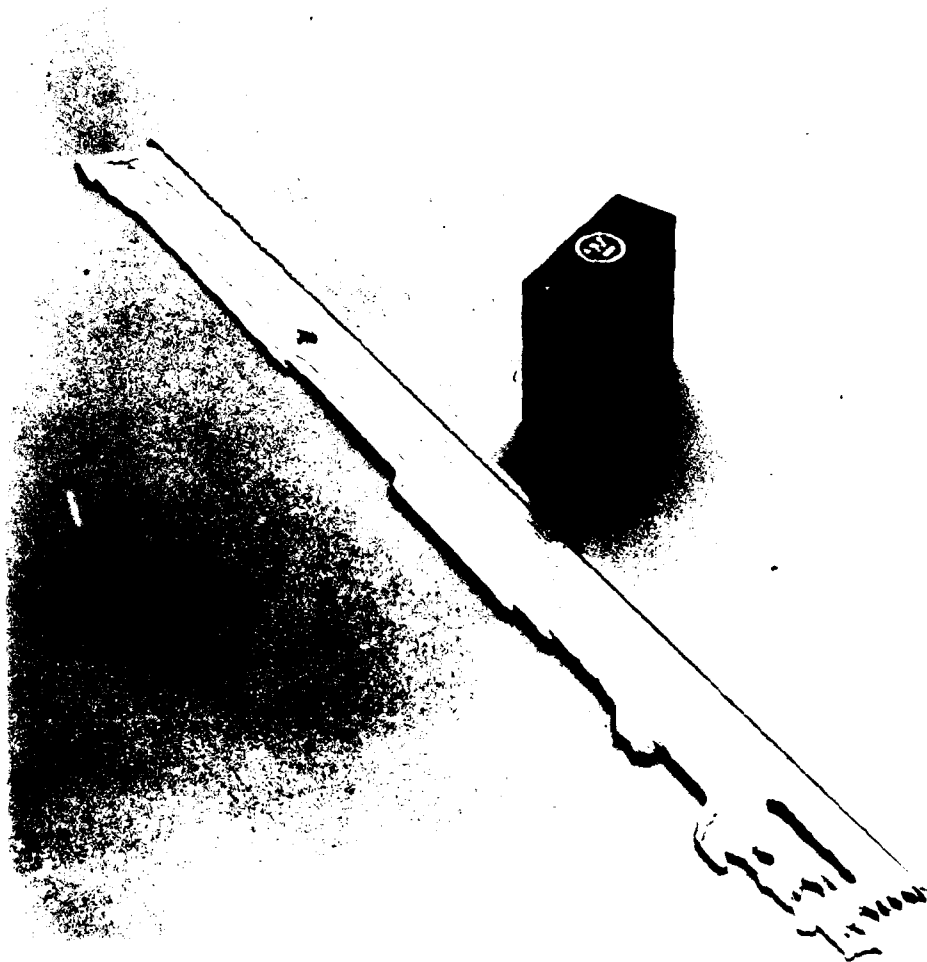


Figure 8 Multidendrite Crystal Having Flat, Faceted Areas.  
These Crystals Grew when Thin Radiation Shields Were  
Incorporated into the Thermal Configuration.

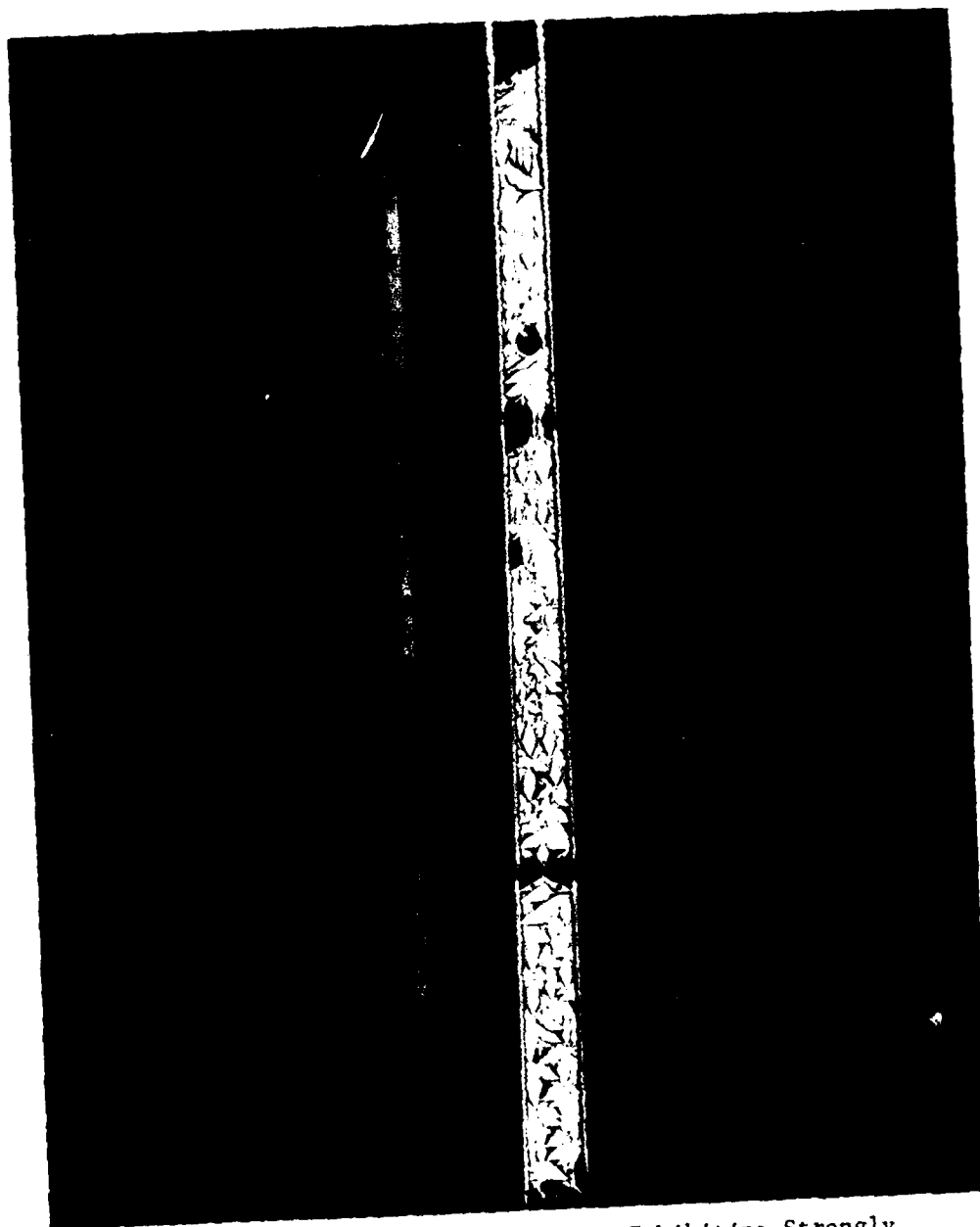


Figure 9 Segment of Te-Doped Crystal Exhibiting Strongly Faceted Web.

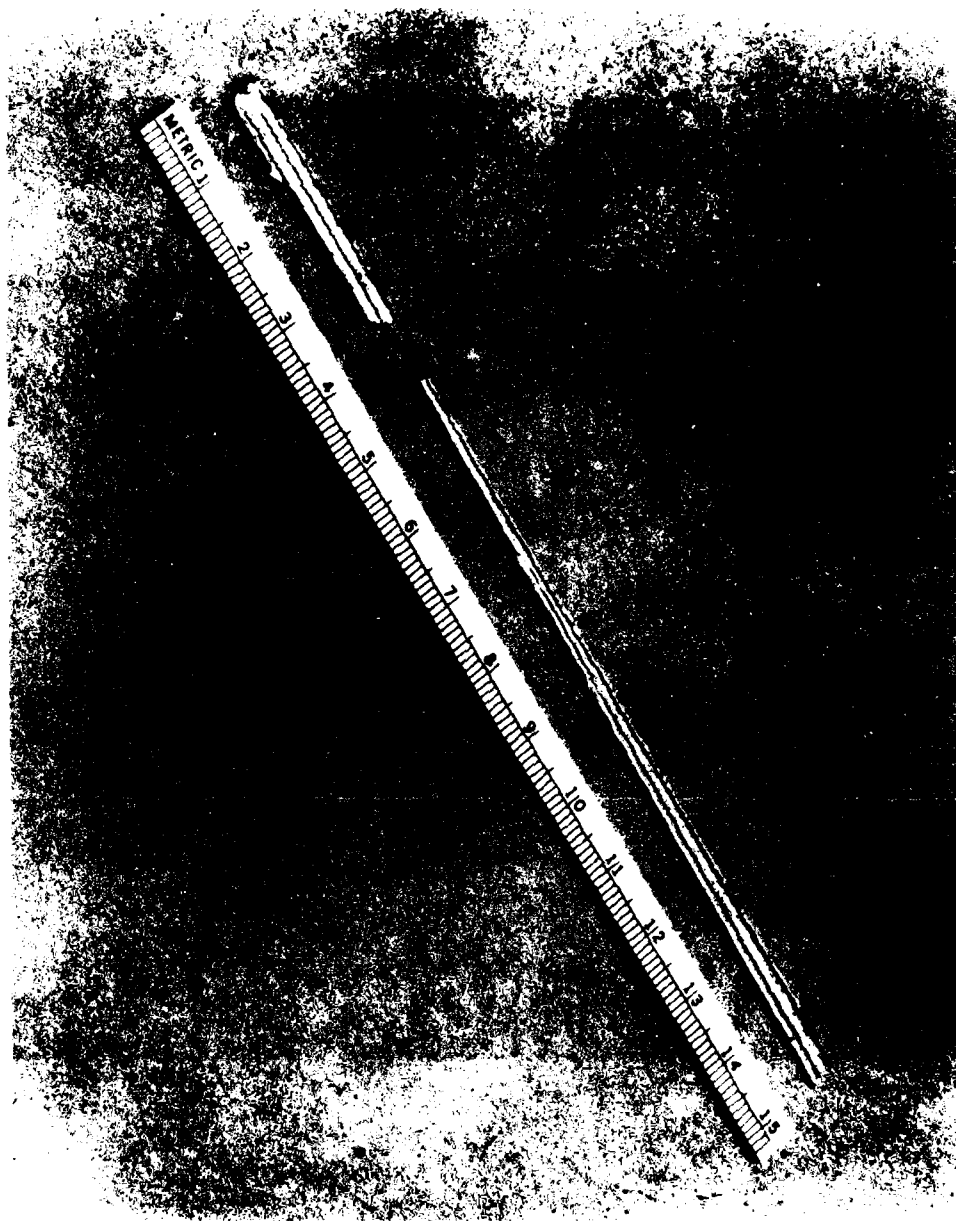


Figure 10 Crystal Grown From a Melt Doped With 1.0 Atomic% Ge. The Ge-Doped Crystals Grew at Low Undercooling and Contained Flatter Textured-Web Areas and Fewer Dendrites Than Typical Undoped or Te-Doped Crystals.



Figure 11 Short Crystal Grown with 0.5 Atomic% Ge Melt Doping.  
The Textured-Web Sections Were the Widest Achieved  
at Small Undercooling,  $<5.0^{\circ}\text{C}$ .

change in growth behavior and ribbon morphology, indicating that the growth kinetics of GaAs play a major role in the multidendrite web structure.

Thermal modification and analysis, seed improvement and characterization, and doping are discussed in the following sections. The results of characterization and orientation analysis are then presented in detail, followed by the concluding discussion.

### 3.2 Thermal Geometry

#### 3.2.1 Thermal Modelling

Successful web growth is critically dependent on the thermal profile in the melt, and this temperature distribution is primarily influenced by the radiative heat exchange between the melt surface and the slot in the lid.<sup>(2,12)</sup> In the GaAs-B<sub>2</sub>O<sub>3</sub> system, the melt-slot radiation exchange is altered by refraction in the B<sub>2</sub>O<sub>3</sub> (Figure 12).

At the inception of the current experiments, the influence of the refractive effect on the temperature distribution in the system was unknown. Therefore, experimentation and thermal modelling were begun in parallel. A system design based on successful Si web systems was used for the initial GaAs growth experiments, and some empirical lid modification was also performed.<sup>(1)</sup> Concurrently, the computerized thermal model that was developed for optimization of Si systems was adapted to model the encapsulated GaAs system.

The thermal analysis yielded the temperature profile in the susceptor/crucible/melt system for a given growth configuration. A finite element technique<sup>(15)</sup> was utilized to perform a steady-state, heat-flow analysis in which conductive and radiative heat transfer were treated. Although some convection was expected, the agreement between modelling and experiment in Si systems indicated that it could be ignored without introducing significant errors into the analysis.

The viewfactors from the melt surface to the slot are ordinarily calculated analytically. The correct viewfactors for radiation refracted and reflected in the B<sub>2</sub>O<sub>3</sub> were obtained by a computerized ray-tracing



Dwg. 7702A32

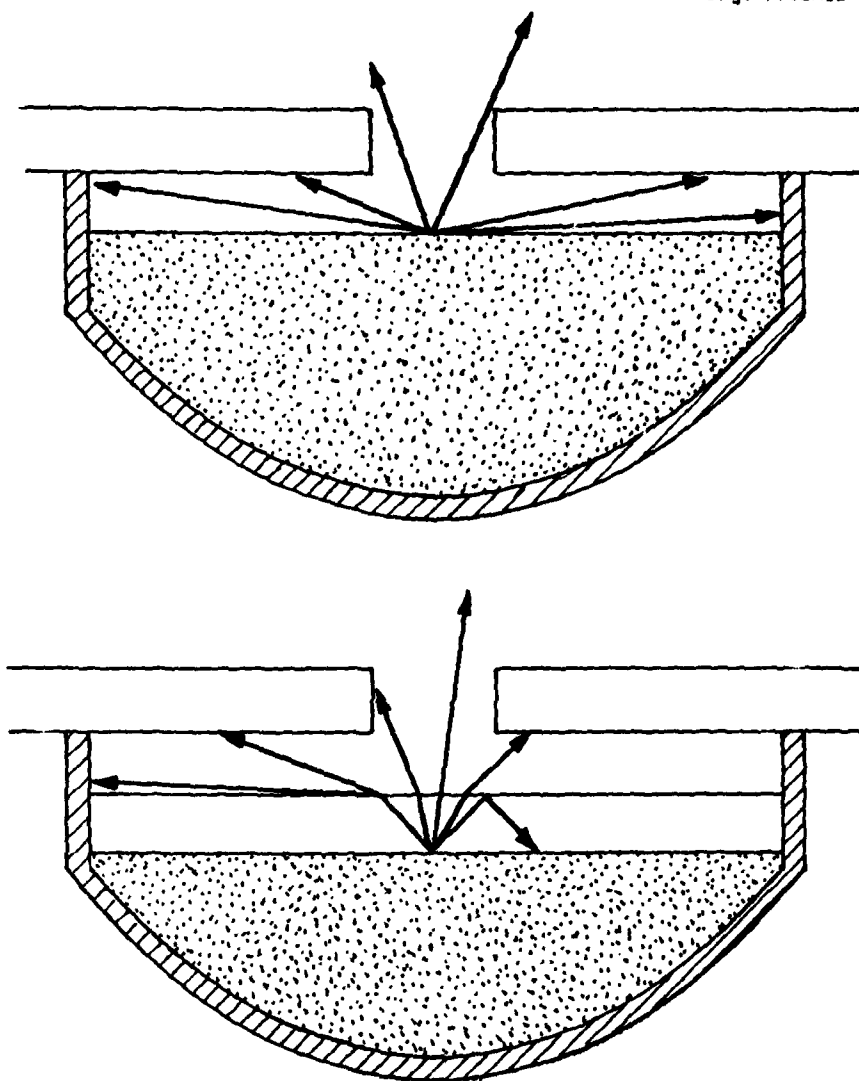


Figure 12 Radiation Exchange Between the Melt Surface and the Lid.  
The Conventional Radiation Exchange (upper figure) was  
Altered by Refraction in the B<sub>2</sub>O<sub>3</sub> (lower figure).

analysis.<sup>(1)</sup> The modified viewfactors were then incorporated into the total heat-flow analysis.

The temperature profiles which were obtained by this method illustrate the thermal effect of the  $B_2O_3$ . The isotherms in the  $B_2O_3$  layer were inverted with respect to the isotherms in the GaAs melt (Figure 13). The model which incorporated susceptor #1 (dashed line in Figure 3) indicated a substantial inversion. This explained a frequent experimental difficulty that occurred when susceptor #1 was in use in which the seed dendrite was severed at the  $B_2O_3$  gas interface. The dendrite melted through in the hotter  $B_2O_3$  even when the melt was undercooled.

Susceptor #2 was designed with no gap below the crucible (full line in Figure 3), thereby transferring heat more effectively into the bottom of the melt. The result obtained by modelling the second susceptor is the profile given in Figure 13. The temperature inversion still occurred; however, the vertical gradient in the encapsulant was reduced by 40%. Also, the horizontal thermal gradient on the GaAs melt surface was reduced by 50%, which is conducive to stable growth of wider-web material.

The modelling results suggested that susceptor #2 produced a substantial improvement in the temperature profiles, and the experimental results reflected this improved thermal geometry. The first GaAs multidendrite web crystal was grown the second time this growth configuration was used (Figure 6), and seed damage in the  $B_2O_3$  was greatly reduced. The new susceptor established a fundamental web-growth thermal geometry, and subsequent thermal "fine-tuning" was performed empirically.

### 3.2.2 Ge Thermal Analog

In addition to computer modelling, we also evaluated the thermal configuration experimentally using a Ge melt. The persistent multidendrite morphology of the GaAs crystals suggested that a detrimental perturbation might be arising from subtle thermal influences or encapsulant interactions. Ge was chosen as an analog material since it grows readily

Dwg. 7721A18

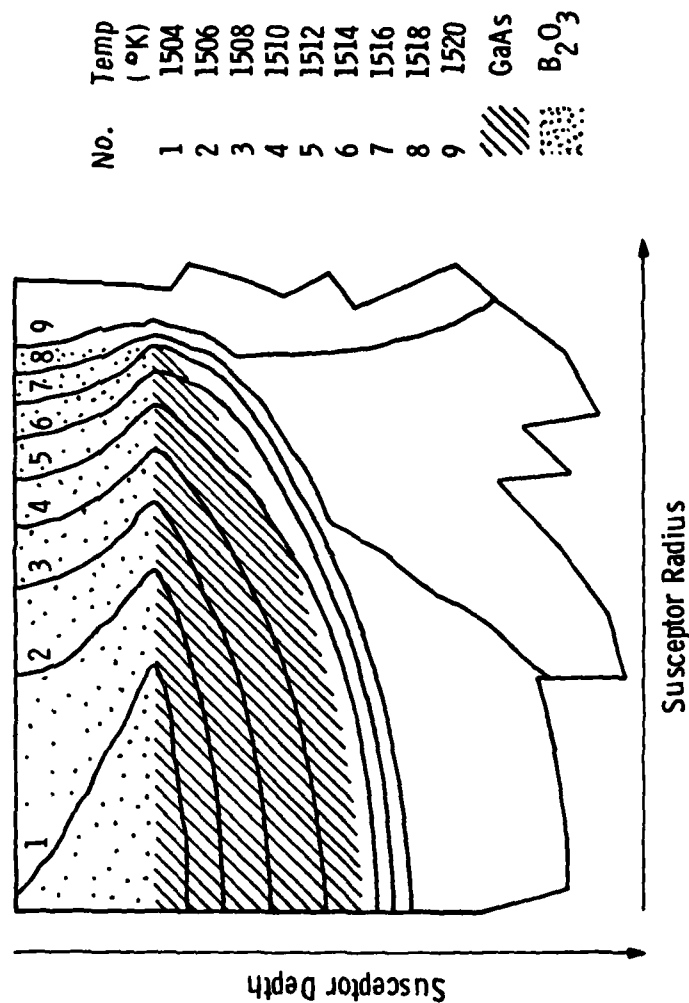


Figure 13 Vertical Thermal Profile for Model Incorporating Susceptor #2. The Profile is a Vertical Cross Section Through the Melt From the Center to the Right Edge, Parallel to the Long Axis of the Slot. Inversion of the Isotherms Occurs at the GaAs-B<sub>2</sub>O<sub>3</sub> Interface.

in a dendritic-web morphology<sup>(16)</sup> and is compatible with the encapsulant. (Si was unsuitable since it reacted with the  $B_2O_3$ .)

The first experiment incorporated a volume of Ge, equal to the typical GaAs volume, without encapsulation. The purpose was to evaluate the overall thermal geometry, particularly the large distance between the melt surface and the lid. In our GaAs system, this gap was generated by the intervening layer of  $B_2O_3$  and by the sinking of the charge into the spherical crucible as it melted. Conventional Ge web (Figure 14) grew from the system, thereby validating the basic growth configuration.

The second Ge experiment included the encapsulant and again, Ge web crystals were grown. Due to the extreme viscosity of the  $B_2O_3$  at the low-growth temperature (937°C), it accumulated on the crystals in a thick layer and shattered the web as it froze. However, the experiment clearly demonstrated the feasibility of conventional web growth through an encapsulant.

The growth parameters of the Ge and Ge- $B_2O_3$  runs reproduced well. In both cases the undercooling required for growth was 5°C and pulling velocities ranged from 1.0-1.6 cm/min. The web thickness measured on recovered fragments ranged over the same values. These results indicated that the addition of the  $B_2O_3$  layer to this system did not appreciably alter the heat transport.

Results obtained with the Ge- $B_2O_3$  system at 937°C were not interpreted rigorously in terms of the GaAs- $B_2O_3$  system at 1238°C since the radiant heat transfer is much greater at GaAs temperatures. However, the experiments demonstrated that there were no pathological problems with the growth system which precluded conventional web growth, and suggested that any remaining thermal alterations required for web growth at 1238°C would be relatively minor.

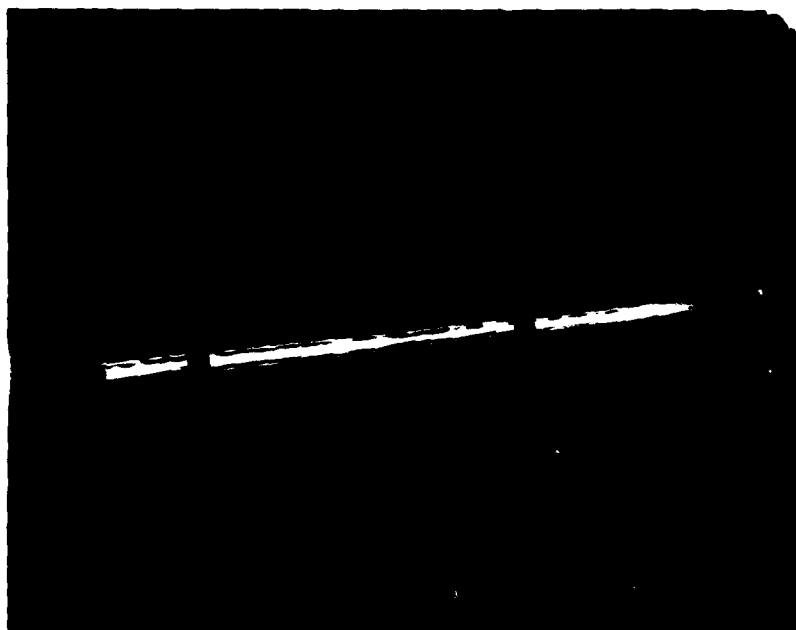


Figure 14 Ge Web Grown from Our System to Test the Viability of the Thermal Geometry for Web Growth.

### 3.2.3 Empirical Thermal Modification and Evaluation

The primary goal of our experimental modifications of the thermal geometry was to reduce the vertical temperature gradient in the melt. The gradient calculated in the model was 60-70% greater than the typical gradient in Si systems, and in the early web-growth experiments, the GaAs crystals did not penetrate and grow unless the melt was undercooled 20-25°C. Si web is typically grown at a melt undercooling of 2-6°C.

The vertical gradient can be adjusted by: 1) vertical positioning of the susceptor with respect to the coil, 2) lid thickness and slot design, and 3) top shields. However, all of these adjustments increased the temperature of the top of the susceptor assembly and thermal damage to the seeds in the slot area, in the cavity above the melt, and in the  $B_2O_3$  limited the latitude and effectiveness of these approaches. A workable thermal geometry evolved in which a 1/8-inch-thick lid (Lid #4) was used with a 1/16-inch-thick shield and two thin radiation shields (Figure 4b) at a very low susceptor position.

The undercooling required for crystal growth dropped to the range of 7-16°C with this configuration and better crystal morphology was obtained (Figure 15). Other growth configurations incorporating "hotter" slot designs or additional shielding produced slightly decreased undercooling (Figure 29, Section VI); however, seed damage precluded their use. We attempted to circumvent this problem by introducing side holes in the susceptor #2 design to cool the  $B_2O_3$ , thereby allowing the use of hotter lids. However, this susceptor modification did not improve the growth behavior of the system.

As experiments with the standard configuration proceeded, the growth behavior suggested that the isotherms in the melt might differ slightly from the calculated profile.  $\langle 211 \rangle$  dendrites branching at 60° to the vertical seemed to be preferred over conventional vertical dendrites as propagation began from the ends of the button. (These  $\langle 211 \rangle$  directions at 60° are allowed growth directions for two-twin-plane



Figure 15 Morphology Comparison of a Crystal Grown with Radiation Shielding (Left) to One Grown Without Radiation Shielding (Right). The Flat, Faceted Areas Resulted From the Improved Thermal Geometry.

dendrites,<sup>(17)</sup> but they should occur with no greater frequency than the vertical  $[2\bar{1}\bar{1}]$ .) This growth behavior suggested that a saddle point might exist in the isotherms rather than the smooth concave profile calculated in the model. Therefore, we evaluated the horizontal profile experimentally.

The apparent shift in the "hold" temperature of a thin seed for several positions on the melt surface along the slot axis gave the horizontal profile. The values in Table 1 show that the profile was very flat and that it corresponded well to the model results, even though changes in lid thickness and shielding had been incorporated into the experimental system.

We concluded that the  $\langle 211 \rangle$  branching was induced by the large undercooling imposed on the flat horizontal gradient, coupled with a steep vertical gradient. Dendrites growing at an angle propagated more easily into the cooler peripheral surface layers than vertical dendrites propagating at greater depth nearer the center.

Seeds with three twin planes and reduced undercooling were sought to remedy the situation. The following sections discuss seed dendrites, and Ge doping (which significantly reduced the undercooling).

### 3.3 Seeds

In addition to a suitable thermal geometry, viable dendrite seeds are required for web growth. Therefore, throughout the program we grew and evaluated dendrites in order to supply seeds for the web-growth experiments.

Ideally, a seed for dendritic web contains an odd number of nondegenerate twin planes (i.e., the twin lamella are not enclosed in the interior of the crystal but continue to the edges) which suppress the growth of branching  $\langle 211 \rangle$  dendrites. Twin-plane degeneracy does not preclude crystal propagation but it is detrimental to seeding.<sup>(17)</sup> Many of our first GaAs dendrites contained degenerate twin planes,<sup>(1)</sup> but nondegenerate twin structures predominated as thermal conditions improved. Also, nearly all the dendrites characterized had an even number of twin planes, usually two.



TABLE 1

## COMPARISON OF THERMAL PROBING AND MODELLING RESULTS

POSITION*	MEASURED VALUE	MODELLED VALUE
7.5mm	$\Delta T_{\infty} 0^{\circ}\text{C} (\pm 1^{\circ}\text{C})$	$1^{\circ}\text{C} \leq \Delta T < 2^{\circ}\text{C}$
15 mm	$\Delta T_{\infty} 2^{\circ}\text{C} (\pm 1^{\circ}\text{C})$	$\Delta T_{\infty} 4^{\circ}\text{C}$

\* Measured from the center along the long axis of the slot.

We attempted to generate odd-twin-plane crystals by a "double-seed" procedure. Two sections of seed were sandwiched together one in the conventional  $[2\bar{1}\bar{1}]$  direction and one in the inverted  $[\bar{2}11]$  direction. (Half of a crystal with an odd number of twin planes grows in the  $[2\bar{1}\bar{1}]$  direction and half in the  $[\bar{2}11]$  direction-see Section V.) In the button of the resultant crystal, both growth directions were present and the boundary between them was coherent over most of its length (Figure 16). However, one growth direction was lost as propagation continued and lower portions of the crystal contained only two twin planes. The "double-seed" approach suffered drawbacks due to the thickness of the seed (see below) and was not pursued.

The "thin-seed" effects observed in the GaAs system were similar to those encountered in silicon web growth. Fine seeds produced thin buttons bounded by extended facets and improved penetration at low undercooling. Conversely, heavier seeds required greater undercooling for nucleation and growth to begin and the buttons were thick and poorly shaped. These effects are apparently governed by the relative proportions of heat loss to the undercooled melt and to the solid via heat flow up the seed stem.

Supplying the web experiments with thin seeds was difficult. Dendrite thickness can be reduced during growth by increasing the pull speed; however, at velocities greater than 3 cm/min, the  $B_2O_3$  was picked up on the growing crystals and cracked them as it froze. The addition of 1 mole% LiF to the encapsulant permitted growth at speeds up to 8 cm/min without accumulation of  $B_2O_3$ ; but initiation of growth was difficult, perhaps due to an etching effect of the LiF. In the latter part of the program, dendrites were thinned for use as seeds by etching with aqua regia.

Characterization studies demonstrated that the twin-plane spacing of crystals often varied considerably from the spacing in the seeds from which they grew. However, as Table 2 indicates, the variation of twin-plane spacing between the top (well under the button) and bottom of individual crystals varied much less. These data suggested that the



Figure 16 "Artificial" Twin Plane (indicated by the arrow) Generated by the "Double Seed" Experiment. Other Twin Structures Visible Were Nucleated From the Two Halves of the Double Seed.

TABLE 2

## VERTICAL TWIN-PLANE CONTINUITY

<u>Twin Spacing Comparison</u>	<u>Average Twin Spacing Variation</u>	<u>Range of Twin Spacing Variation</u>
Seed vs Crystal	28%	1% - 125%
Crystal Top vs Crystal Bottom	7%	0.07% - 37%
Seed vs Button	7%	2% - 11%

twin structure of the seeds was not being propagated into the crystals, perhaps due to thermal damage to the seeds.

Several buttons with seed remnants still attached were mounted and polished in steps to "track" the twin structure from the seed into the button. We found that the twin spacings in the top of the button corresponded well to the seed-twin spacing (Table 2). However, polishing farther into the buttons revealed that the twin structure often changed with depth in the button. Twin-structure aberrations are discussed further in Section VI in the context of interface stability.

### 3.4 Doping Effects

Doping capability is required to produce suitable GaAs base material for solar cells, therefore it was tested in the liquid-encapsulated-system. Also, heavy doping increased the proportion of odd-twin-plane structures in Ge dendrites,<sup>(17)</sup> thus we sought a similar effect in our GaAs crystals. Te doping at melt concentrations of  $5 \times 10^{18}/\text{cm}^3$  produced n-type crystals and slightly increased the proportion of three-twin-plane material.

The most dramatic doping effects resulted from the addition of 0.3-3.0 atomic% Ge to the melt. The motivation for these experiments was to probe the inherent materials influences of GaAs on the growth behavior and morphology of web crystals via chemical modification. Ge was chosen for this purpose because of the excellent size match of the Ga, Ge, and As covalent radii.

The addition of 3.0 atomic% Ge to the melt 1) reduced the undercooling to the range of 2-7°C (Figure 29 in Section VI); 2) improved the web morphology (Figures 17 and 18); and 3) suppressed the formation of surface Ga droplets (Figure 19). However, 1.0-3.0 atomic% Ge melt doping produced internal Ge inclusions in the grown crystals. Reduction of the melt doping to 0.5 atomic% Ge prevented phase separation, but the crystal surfaces were again degraded with Ga droplets.

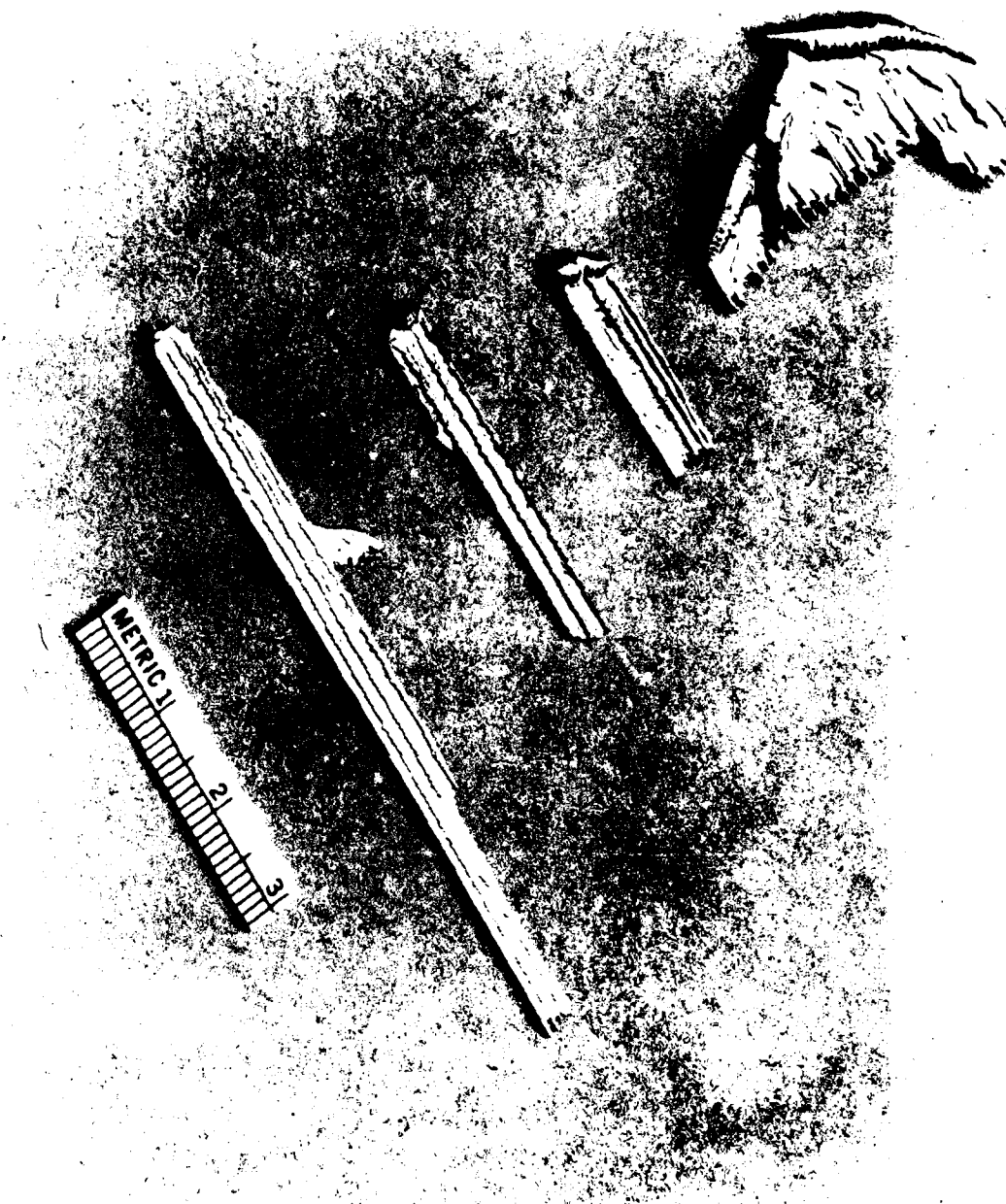


Figure 17 Comparison of Three Ge-Doped Crystals (left) to an Undoped Button (right). The Faceted Morphology was Improved and Branching Growth was Reduced in the Narrow Ge-Doped Crystals.

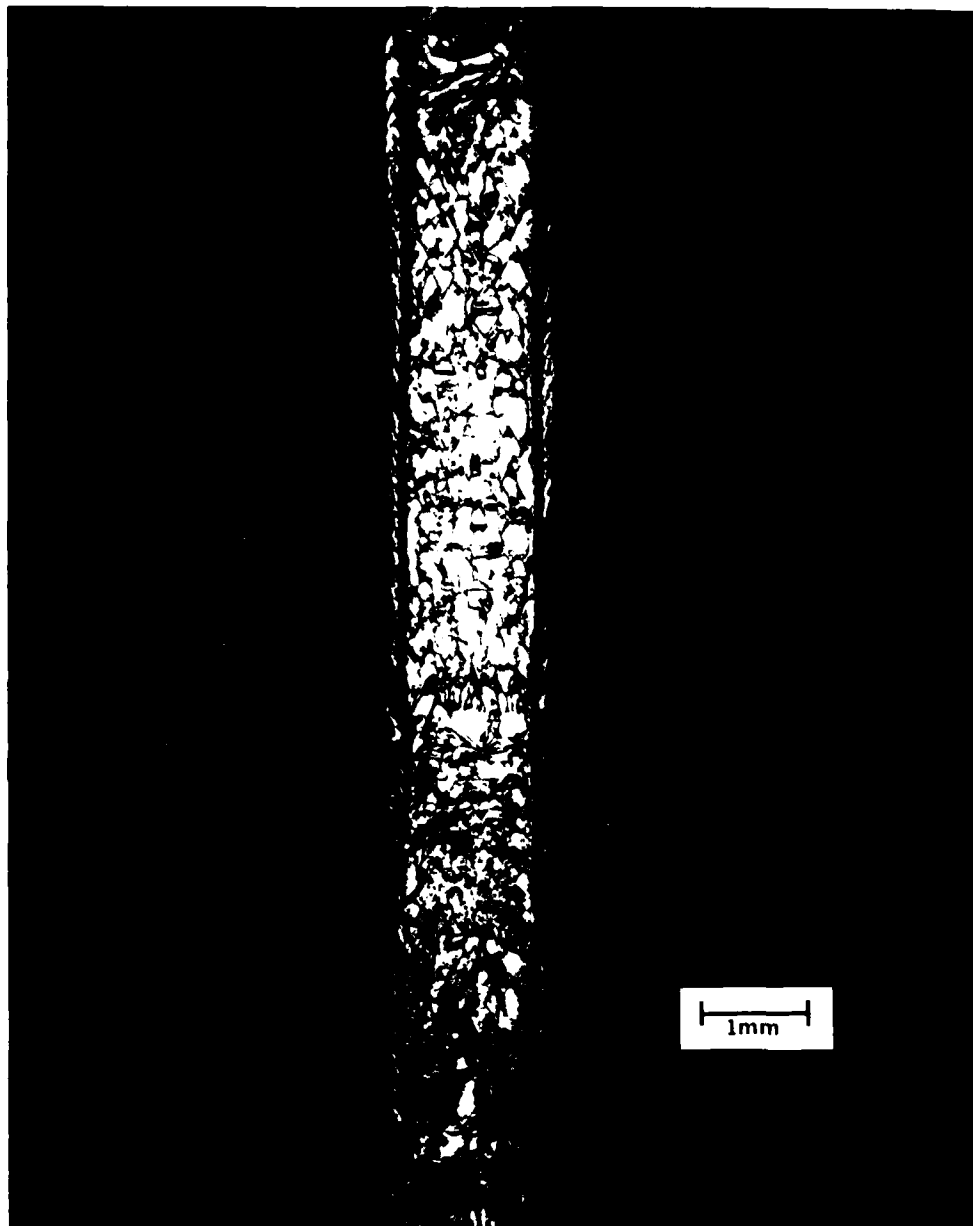


Figure 18 Close-up of Ge-Doped Textured Web which was Composed of Small Facets.



Figure 19 Comparison of a Typical Crystal Surface Marked by Ga Droplets Running in the Growth Direction (upper photo) With Surface of a Crystal Grown With 3.0 Atomic% Ge-Melt Doping (lower photo).



The marked changes in the growth habit of Ge-doped crystals are illustrated in Figure 17, which compares short segments of doped crystals with an undoped button. The Ge-doped buttons and crystals were narrower, but the propagation of branching growth was reduced and the overall web morphology was improved. A large percentage of the Ge-doped crystals contained more extensive web areas (in proportion to the overall crystal size) and fewer dendrites than other crystals. On close examination the flat, textured web areas were composed of small facets, as illustrated in Figure 18.

The morphological improvements of Ge-doped webs are consistent with the reduced undercooling at which the crystals grew. However, there was not a simple cause and effect relationship between the improved crystal quality and the reduced undercooling. When the Ge doping level was reduced to 0.5 atomic% (melt doping) the occurrence of multidendrite morphology increased despite the fact that the undercooling remained  $\leq 5.0^{\circ}\text{C}$ . Therefore, the morphology was *directly affected by the Ge content* as well as by the reduction in undercooling which the Ge doping produced.

## SECTION IV

### CHARACTERIZATION

#### 4.1 General Description

The GaAs multidendrite web crystals grown during Phase II ranged in length from 1.2 cm to over 30.0 cm which was the pulling limit of the apparatus (Table 3). The width was typically  $\geq 1.5$  cm for conventional crystals and  $\leq 1.0$  cm for Ge-doped webs. The thickness of individual crystals varied over their widths due to the multidendrite structure, and thickness measurements were therefore made both on the heavy dendrite areas and on the thinner web areas of the samples. The Ge-doped crystals contained significantly thinner dendrite areas than the undoped and Te-doped samples. The web areas of the crystals were 100-300  $\mu\text{m}$  thick, which is comparable to typical Si-web thickness.

The crystals grew in the conventional  $[2\bar{1}\bar{1}]$  direction and developed (111) faces (Figure 1). Because GaAs crystallizes in the zinc-blende structure, one ribbon face was composed of (111) Ga planes, while the opposite face was composed of (111) As planes.<sup>(18)</sup> (This is true independent of the number of twin planes since the twinning operation is a rotation about the  $[111]$  direction.)

The tartaric acid etch (Section 2.3) designated the Ga face; morphological differences in the faces, however, usually allowed visual identification. For the conventional  $[2\bar{1}\bar{1}]$  growth direction, the Ga face exhibited steep "arrowhead" facets which were absent from the As face (Figure 27, Section V.) Also, the Ga face of single dendrites was narrower than the As face as reported by previous authors.<sup>(19)</sup>

TABLE 3  
CRYSTAL DIMENSIONS

	Undoped and Te-Doped	Ge <sup>*</sup> Doped
Length		
Range	4.0 - 31.0 cm	1.2 - 22.0 cm
Average	$\geq 15.0$ cm	$\leq 10.0$ cm
Width		
Range	0.3 - 3.0 cm	0.6 - 1.7 cm
Average	$\leq 2.0$ cm	$\leq 1.0$ cm
Thickness		
Dendrite Areas	400 - 800 $\mu\text{m}$	300 - 500 $\mu\text{m}$
Web Areas	100 - 300 $\mu\text{m}$	100 - 300 $\mu\text{m}$

\*The dimensional peculiarities of the Ge-doped crystals reflect the small undercooling at which they grew.

Another feature of the GaAs webs was the frequent occurrence of branching dendrites at  $60^\circ$  to the vertical. The branching growth dominated buttoning at large undercoolings (Figures 11, 17) and also occurred spontaneously off the ribbon edges at any point during growth (Figure 7).

The rough, textured surfaces of the multidendrite crystals had the appearance of polycrystalline web. However, throughout the program several samples (both doped and undoped) were x-rayed and yielded single-crystal (111) Laue patterns with no distortion or splitting of the spots. The triangular etch pits produced by the tartaric acid etch pointed in the  $\langle 2\bar{1}\bar{1} \rangle$  directions and provided a straightforward optical test for facet orientation. The etch pits remained aligned across facet boundaries of the crystals which were tested, as illustrated in Figure 20.

The flatter, textured web areas of a Ge-doped sample were examined with the SEM. Some facets formed periodic web sections bounded by flow lines originating at the side dendrites; other web facets were bounded by sharp crystallographic planes as shown in Figure 21.

#### 4.2 Twin Structure

The twin structures of 67 GaAs dendrites and webs were analyzed on mounted cross sections. The spacing varied widely (Table 4) and was generally larger than the spacing typical of Si web. Only a few Ge-doped crystals were analyzed, but most of the measurements fell in the reduced range of 6.0–10.0  $\mu\text{m}$ .

In addition to the larger spacing, the GaAs twin structure differed from Si-web twin structure in several other ways. All but seven of the 67 crystals that were characterized contained an even number of twin planes, usually two, while Si web is grown with three twin planes. (The difficulty of growing three-twin-plane GaAs web is discussed further in Sections V and VI.) There was also a strong tendency for the GaAs twin planes to degenerate. Although twin-plane degeneracy was reduced with improved thermal conditions,  $\sim 35\%$  of the cross sections taken from

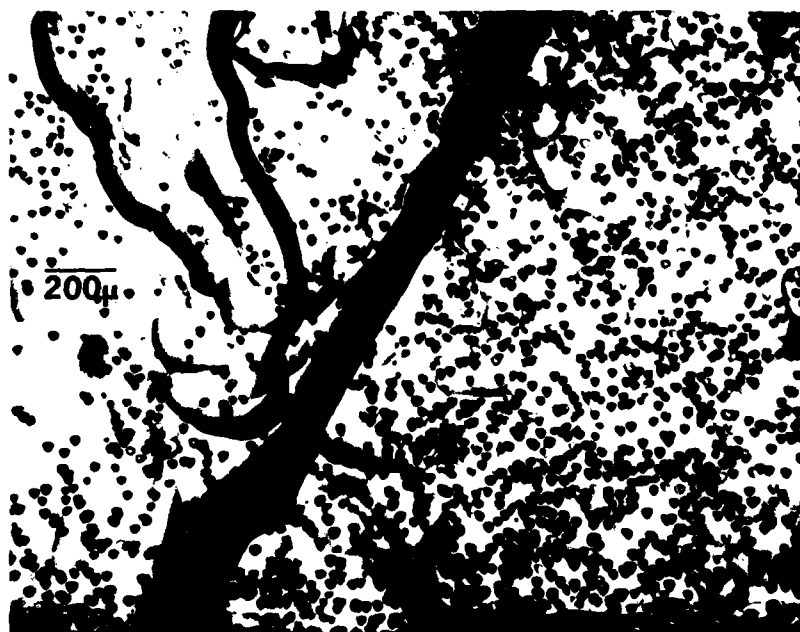


Figure 20 Optical Micrograph of Surface Facet Orientation. The Triangular Etch Pits which Point the  $[2\bar{1}1]$  Direction Remained Aligned Across Facet Boundaries.

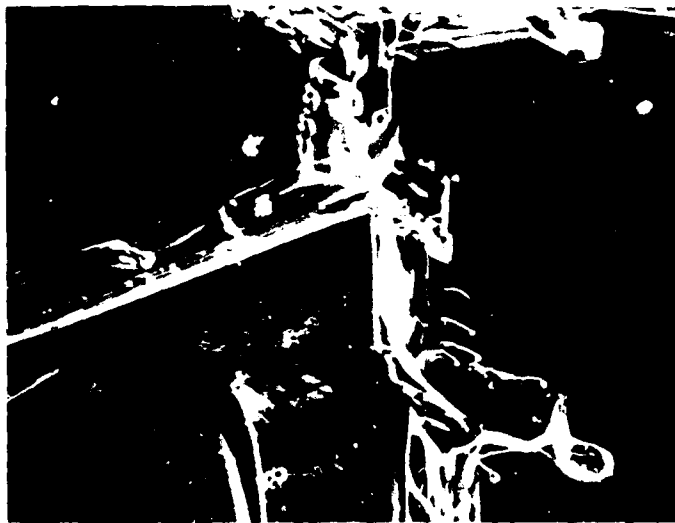


Figure 21 SEM Micrographs of Surface Facets on a Ge-Doped Crystal. In Some Areas Flow Boundaries Formed Regular Patterns (upper photo). In Other Areas the Facets were Bounded By Crystallographic Planes (lower photo).

TABLE 4

TWIN-SPACING SUMMARY

Range	0.1 $\mu\text{m}$ - 33.8 $\mu\text{m}$
-------	--

Typical Values

Undoped or Te-doped	3 $\mu\text{m}$ - 15 $\mu\text{m}$
------------------------	------------------------------------

Ge-doped	6 $\mu$ - 10 $\mu$
----------	--------------------

material grown in the latter part of the program contained degenerate twin planes. In addition, nondegenerate twin structures often contained steps or jogs.

#### 4.3 Composition

As Figure 19 illustrates, the surface facets of the dendrites and web material were marked with small droplet features that ran in the growth direction. Electron dispersive analysis indicated that the drops were pure Ga, while the disturbed surface behind the drops and the smooth regions (area 1, Figure 22) were stoichiometric GaAs. The Ga phase accounted for less than 5% of the surface area and did not appear to affect the body of the material.

Crystals that accumulated  $B_2O_3$  during growth did not exhibit these Ga droplets. We also observed occasional droplet features which left depressions bounded by crystallographic planes (Figure 22). Both of these effects suggested that the Ga droplets formed at the surface of the crystal after it was completely solidified and was above the  $B_2O_3$ .

The following sequence of events resulting in the droplet surface features was envisaged. The growing material was exposed to a very hot environment until it was pulled above the lid. As it traversed the hot cavity, local As loss at the surface produced a small pool of Ga. Driven by the steep temperature gradient, the Ga moved toward the melt,<sup>(20)</sup> leaving a trail of stoichiometric material. As the crystal was pulled above the lid, the temperature dropped; GaAs dissolved in the pool froze and expanded, forcing the Ga phase out from the surface in a droplet shape.

The cooler radiation shields that overhung the slot did not noticeably improve the surface of the crystals. Apparently, the As loss occurred before the slot region was reached in the hot cavity between the melt surface and the lid.





Figure 22 SEM Photo of Droplet Formation Yielding Depressions Bounded by (111) Planes. The Droplets are Pure Ga, but the Trails and Depressions and the Smooth Regions (area 1) are Stoichiometric GaAs.

A substantial reduction in the surface degradation was observed for crystals grown from melts doped with 3.0 atomic% Ge, as discussed in the previous section. The mechanism of this Ge effect was not investigated.

#### 4.4 Dislocations

During the first half of Phase II, we determined the surface-dislocation density on several GaAs dendrite and web samples using the AB etch to clean the surface and the tartaric acid etch to produce etch pits at dislocations (Section 2.3). The surface-dislocation density varied considerably from one sample to another and also varied between different areas of a given sample.

Typically, dislocation densities ranged from  $10^2/\text{cm}^2$  to  $10^3/\text{cm}^2$ , with isolated regions having densities at least an order of magnitude higher.

Frequently, the dislocations were scattered and bore no apparent relationship to surface features caused by the Ga droplets (Figure 23). In less than half the dendrites examined, dislocations were preferentially located along the central axis, sometimes in clusters. These clusters of dislocations may have resulted from trapping of liquid droplets during growth. (17)

Several samples exhibit the increased dislocation densities in "transition" areas. For example, a high-dislocation density occurred on one sample on the flat web surface directly below the button. Several other specimens exhibited increased dislocation densities in regions where a dendrite became distinguishable from the button and began to propagate.

#### 4.5 Electrical Properties and Impurities

Electrical measurements were performed on several multidendrite web samples. A measurable p-type conductivity was indicated by four-point probe measurements on undoped samples despite the semi-insulating character of the starting material. Te-doped samples were n-type and Ge-doped samples were p-type, as expected.



Figure 23 Typical Dislocation Density and Distribution in GaAs Dendrite and Web Samples.

Hall measurements obtained for one early web sample confirmed the p-type conductivity of the undoped material. Values for mobility and carrier concentration were calculated under the assumption that the sample was electrically homogeneous throughout its thickness. We obtained carrier concentrations of  $4 \times 10^{15}/\text{cm}^3$  at room temperature and  $7 \times 10^{13}/\text{cm}^3$  at 77°K. Mobility values of 44  $\text{cm}^2/\text{v-sec}$  and 410  $\text{cm}^2/\text{v-sec}$  were obtained for room temperature and 77°K, respectively.

We did not investigate the low mobility and p-type conductivity of the undoped samples in detail, however, SIMS<sup>+</sup> impurity analyses were obtained for several samples. The SIMS results indicated the presence of acceptors such as Mn and Fe in concentrations of  $1 \times 10^{15}/\text{cm}^3$  to over  $1 \times 10^{17}/\text{cm}^3$ . Uncalibrated mass spectral scans were also obtained for a web sample and its starting material to compare the impurity content for mass ranges 1-30, 60-67, and 190-200. Although concentration values were not obtained, normalization of the spectra provided an intensity comparison. The web sample contained slightly greater amounts of Si (from our quartz crucible-the starting material was compounded in a PBN crucible) and exhibited an extremely small Pt signal which was absent from the starting material spectra. The latter was probably introduced by the Pt-Au crucible in which the  $\text{B}_2\text{O}_3$  was dried prior to use. All other variations between the two spectra were within the error bars of the measurement and we concluded that our web growth system did not significantly increase the impurity content of the GaAs above the levels present in the starting material.

<sup>+</sup>The SIMS analyses were performed by Charles Evans and Associates, San Mateo, CA using a Cameca IMS-3F ion microanalyzer.

## SECTION V

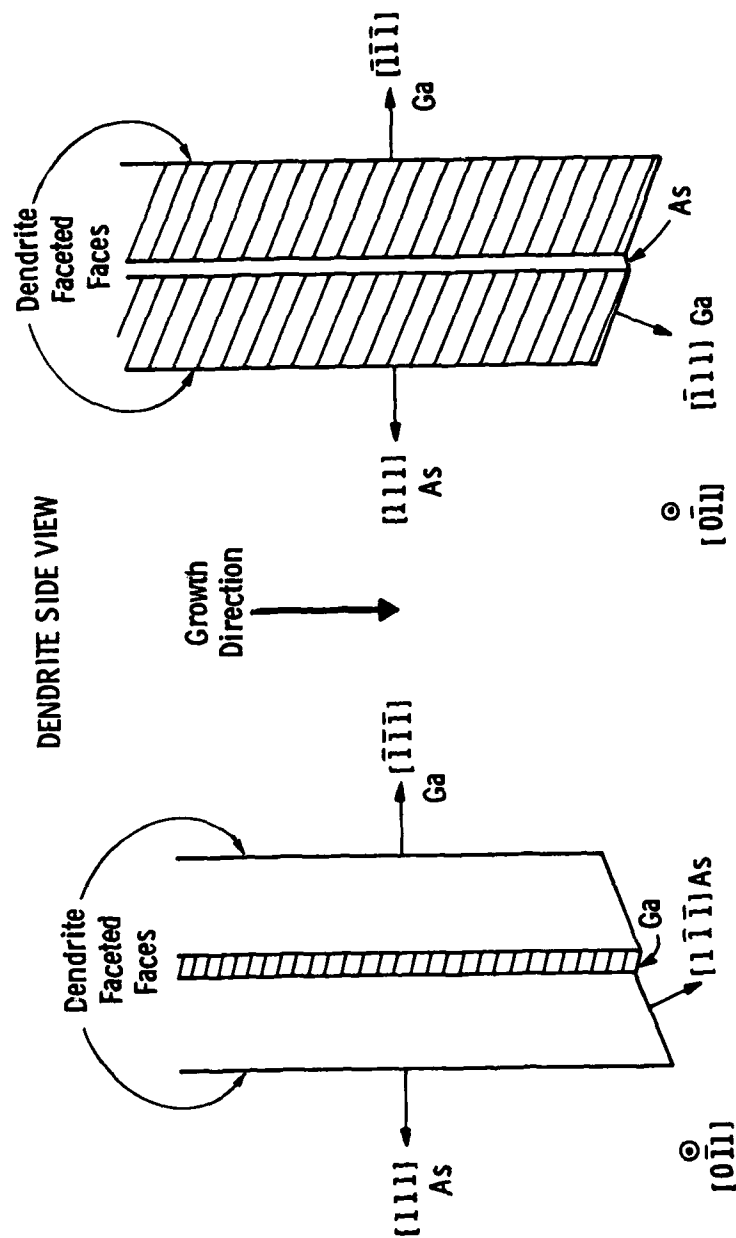
### ORIENTATION ANALYSIS

The unconventional morphology of our GaAs crystals prompted us to investigate the orientation relationships of GaAs dendritic growth. In the qualitative model of Si-web growth, (111) facets bound the growth interface<sup>(21)</sup> (Figure 31, Section VI). The (111) planes of GaAs are polar planes and their influence on the dendrite face morphology has already been described. If polar (111) facets occur at the growth interface of GaAs dendritic web, they may influence the growth behavior. Therefore, we examined orientation relationships in detail.

We assumed that a faceted interface exists for GaAs and determined the bounding planes. For two twin planes (the structure that predominated in our crystals), dendritic growth in the  $[2\bar{1}\bar{1}]$  direction must occur on an As<sup>\*</sup> plane over the majority of the interface, as Figure 24 shows. Dendritic growth in the  $[\bar{2}11]$  direction, however, must occur on an interface that is primarily a Ga plane.

The  $\text{HNO}_3$  twin-plane etchant (Section 2.3) illustrated these orientation relationships. Figure 25 is an SEM photo of an etched cross section of a four-twin-plane dendrite. The  $[2\bar{1}\bar{1}]$ -twinned areas etched more slowly than the surrounding  $[\bar{2}11]$  material, producing two raised steps which bordered on each other. These steps were bounded by a vertical wall on one side (bright line in photo) and a shallow sloping wall on the other (dark bands in photo).  $\text{HNO}_3$  etchants for GaAs reveal As faces; therefore, the bounding surfaces of the raised twinned areas are the nearest As planes. Figure 26 gives a schematic side view of the cross sections to illustrate the relationship between the etch pattern

\*  $\langle 111 \rangle$  directions are designated as Ga or As according to the notation of Dewald.<sup>(22)</sup>



  $[\bar{2}1\bar{1}]$  Growth Direction  
  $[\bar{2}11]$  Growth Direction

**Figure 24** Orientation Analysis of GaAs Web Assuming a Faceted Interface. The  $[2\bar{1}1]$  Growth Direction is Bounded by an As  $[\bar{1}\bar{1}\bar{1}]$  Plane. While the  $[\bar{2}11]$  Growth Direction is Bounded by a Ga  $[111]$  Plane.



Figure 25 SEM Photo of Etched Four-Twin-Plane Cross Section. The Raised Steps are the  $[2\bar{1}\bar{1}]$  Twinned Sections which were More Etch Resistant Than the  $[\bar{2}11]$  Crystal. Each Twin was Bounded by One Vertical Step (right line) and One Shallow Step (dark band) which Delineate the Closest  $\{111\}$  As Planes (see Figure 26).

Dwg. 7746A83

# DENDRITE SIDE VIEW

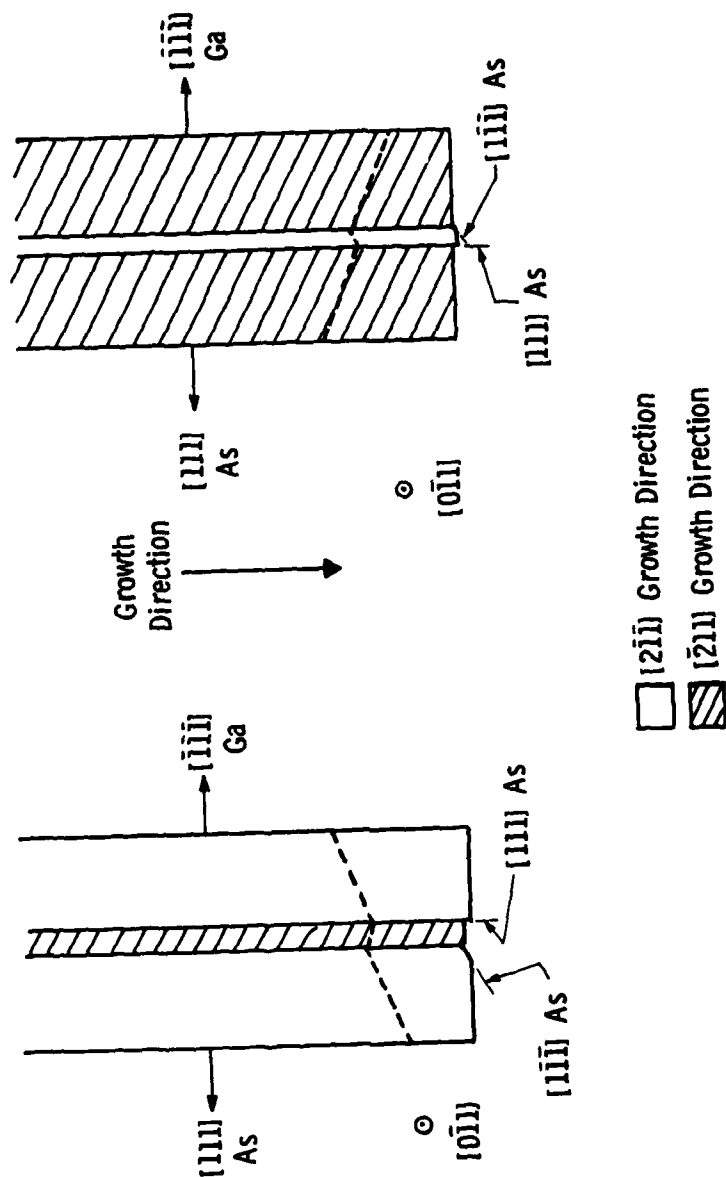


Figure 26 Schematic Section of  $\text{HNO}_3$  Etchant Effect Illustrating the As Planes which Form the Twin Boundaries. Compare the Right-Hand Section to Figure 25.



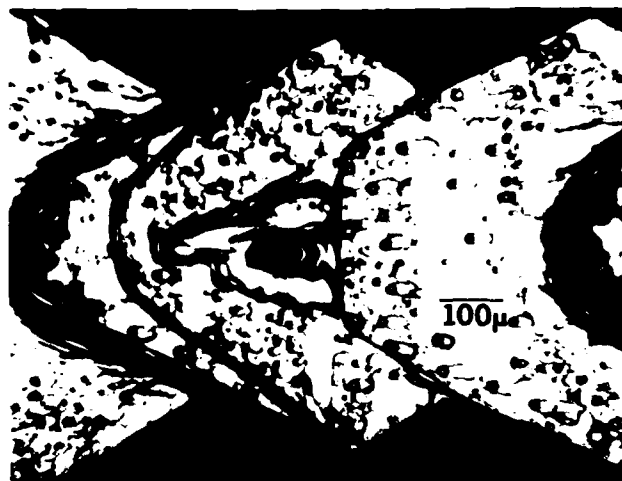
and the orientation of the  $\{111\}$  planes. ( $[2\bar{1}\bar{1}]$  cross sections examined with the SEM exhibited a depressed twinned area with one vertical and one sloping wall, as Figure 26 indicates.) Once this relationship was established, the cross-section etch pattern provided a double check on other etching methods used to determine crystal orientation and the number of closely spaced twin planes.

A three-twin-plane crystal requires that half of the crystal grows in the  $[2\bar{1}\bar{1}]$  direction and half in the  $[\bar{2}11]$  direction. All of our early two-twin-plane crystals grew in the  $[2\bar{1}\bar{1}]$  direction--suggesting that perhaps the  $[\bar{2}11]$  direction was difficult to propagate--thereby precluding the growth of three-twin-plane crystals. Subsequently, inverted seeds produced  $[\bar{2}11]$  growth with equal ease, although the morphology of the dendrite faces differed with growth direction.

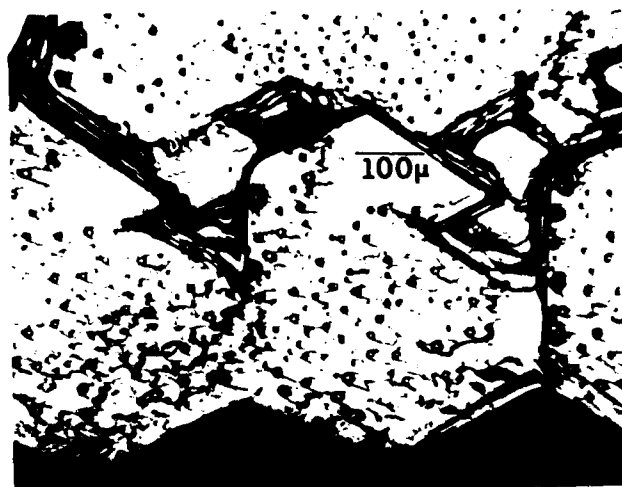
For  $[2\bar{1}\bar{1}]$  crystals, the Ga face exhibited prominent arrowhead-growth steps, while the As face was much flatter and creviced with an obscure interlocking pattern (Figure 27a&b). Conversely,  $[\bar{2}11]$  crystals exhibited poorly defined arrowhead facets--often forked, as shown in Figure 27c--on the flat As face, and well-defined hexagons on the Ga face (Figure 27d). All of these shapes can be derived from the equilibrium GaAs crystal bounded by both Ga and As  $\{111\}$  faces (Figure 27e). However, the variation of morphology with growth direction confirms the influence of the polar planes on dendritic growth behavior of GaAs.

Analysis of the few three-twin-plane crystals that were grown yielded additional intriguing results. There are two possible interfaces for three-twin-plane crystals, depending on the relative position of the  $[2\bar{1}\bar{1}]$  and  $[\bar{2}11]$  sections of the crystal (Figure 28). The web interface dominates Si-dendrite growth and is the only observed interface in Si-web growth. However, for five GaAs crystals that had three twin-planes, three grew with the inverted interface and only one with the web interface. The fifth crystal exhibited both interfaces in different sections that had propagated from different areas of the button.

(A)



(B)



(C)



Figure 27A-C Morphology Comparison of Ga and As Faces of  $[2\bar{1}1]$  and  $[\bar{2}11]$  Dendrites; Growth Direction to the Left. A)  $[2\bar{1}1]$ , Ga Face; B)  $[2\bar{1}1]$ , As Face; C)  $[\bar{2}11]$ , As Face.

(D)



(E)

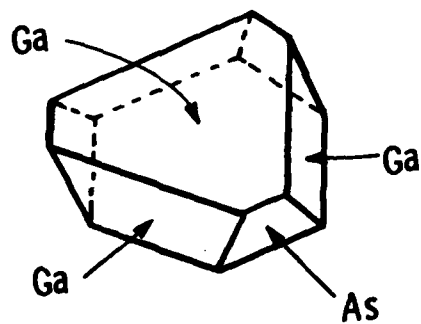


Figure 27D,E D)  $[\bar{2}11]$ , Ga Face; E) Equilibrium Form of GaAs Crystal Bounded by Both Ga and As  $\{111\}$  Planes.

Dwg. 7746A84

### 3 TWIN PLANE INTERFACE TYPES

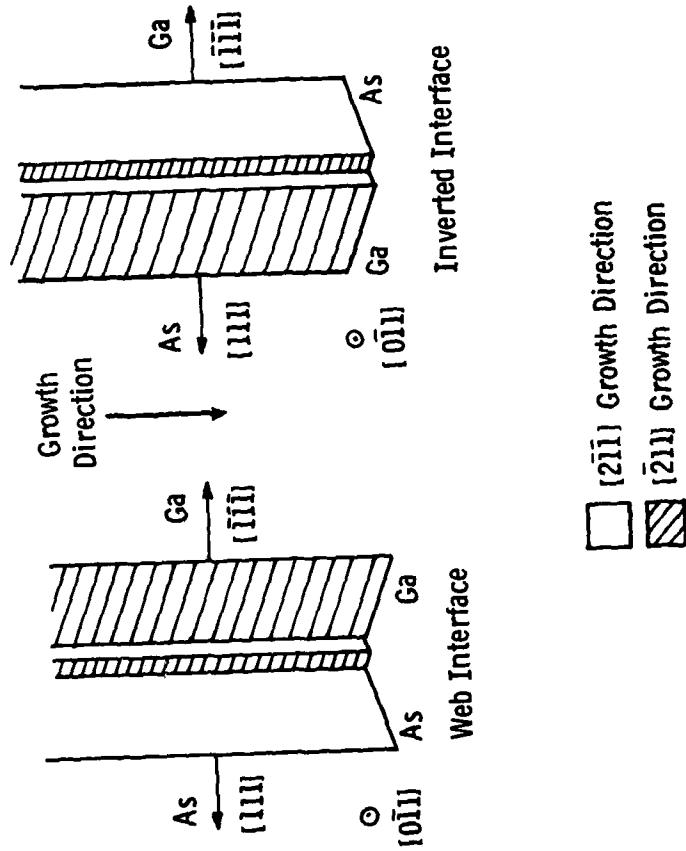


Figure 28 Possible Three-Twin-Plane Interface Types. For Si Web, Only the Web Interface is Observed. The Inverted Interface Predominated in Our GaAs Crystals.

The occurrence of both three-twin-plane interface types in GaAs may explain why branching  $\langle 211 \rangle$  dendrites were not totally suppressed in these crystals. For a three-twin-plane crystal growing vertically with the web interface, the branching directions must have the inverted interface. Therefore, in Si, where the inverted interface does not grow, the branching  $\langle 211 \rangle$  directions are suppressed. However, for our GaAs crystals, both interface types were allowed and branching growth was therefore not eliminated even in three-twin-plane crystals.

The three-twin-plane structure of GaAs webs also had a strong tendency to degenerate to a two-twin-plane structure throughout the length of the crystal. In every case in which a twin plane became incoherent and "grew out" of the crystal, it resulted in an overall  $[\bar{2}11]$  growth direction.

The preference for the Ga bounded interface (Figure 28) under these circumstances suggests that the polar nature of GaAs influences dendritic web growth behavior at a very fundamental level.

## SECTION VI

### CONCLUSIONS

The web-growth results of the program strongly suggest that the unconventional growth behavior and morphology of GaAs web result primarily from fundamental materials properties. The thermal geometry and seed quality also influenced the crystal-growth results, but chemical modification of the melt had the most dramatic impact on the growth parameters and on the web morphology. For example, Figure 29 illustrates the effect of both thermal and chemical changes on the undercooling required for growth. Ge doping produced by far the largest effect, reducing the undercooling into the conventional range.

Prior to the Ge-doped experiments, we had assumed that the unusual morphology of the crystals was induced by the large undercooling. Although the morphology improved at low undercooling, multidendrite structures still formed frequently and web areas were textured with small facets.

Unconventional twin structures were also characteristic of the GaAs crystals. Instabilities in the twin structures (Figure 30) often developed during buttoning, producing discontinuities between twin spacings in crystals and their seeds and frequent degeneracies. Three-twin-plane structures were extremely rare; those that grew usually exhibited the inverted interface rather than the web interface and degenerated to two-twin-planes, producing a  $[\bar{2}11]$  growth direction.

All of the evidence summarized above indicates that GaAs dendritic-web growth processes differ from those in Si. A rigorous theory of Si dendritic-web growth has not been developed; plausible qualitative growth models, however, suggest that atomic attachment processes play a crucial role in stable web propagation.

## UNDERCOOLING FOR CRYSTAL GROWTH VS THERMAL AND DOPING CONDITIONS

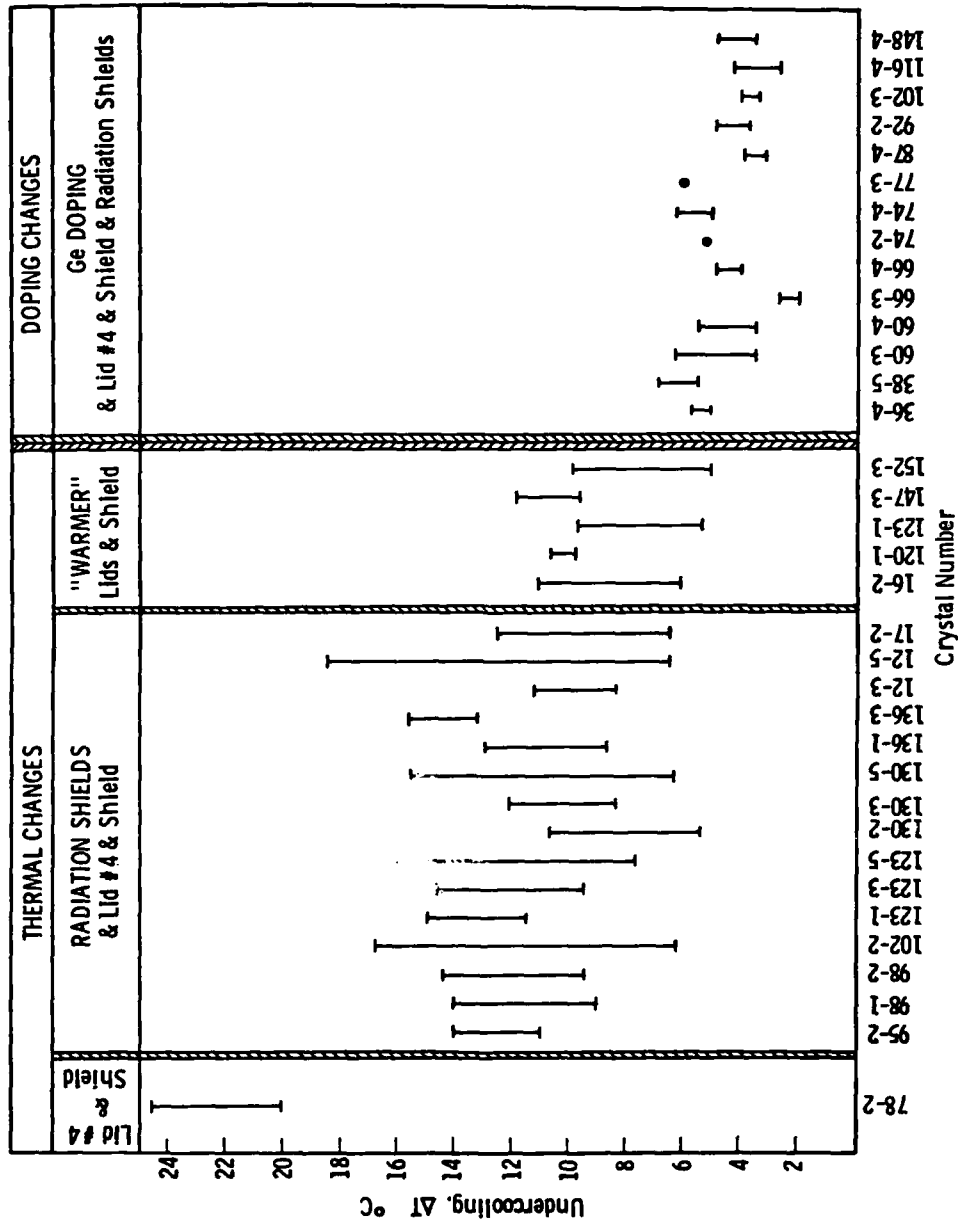


Figure 29 The Influence of Thermal and Doping Changes on the Undercooling Required for Growth. (Data Show the Undercooling Range Experienced By a Crystal During Growth, Not Error Bars.) Thermal Modifications Reduced the Undercooling but "Warmer" Lids and Shields Caused Seed Damage. Conventional Undercooling Values Were Achieved Only With Ge Doping.



Figure 30 Twin-Structure Breakdown in a Three-Twin-Plane GaAs Button Polished Vertically From the Seed to a Depth of 1.3cm. Twin Planes Developing Incoherent Loops Above Were Lost From the Crystal in Subsequent Sections.



We assume that the Si web interface is stable in the presence of an undercooled melt because it is faceted. Pronounced (111) faceting in Si indicates that atomic attachment is difficult on (111) planes. Thus, nucleation on the faceted interface is unlikely, while corner nucleation at the intersection of the web and bounding dendrite is energetically more favorable. Forward propagation occurs by rapid lateral growth across the interface once a layer is nucleated, as illustrated in Figure 31.<sup>(21)</sup>

One might expect the twin structure of the web to provide a mechanism for spontaneous dendrite growth from the interface by the reentrant corner mechanism that is responsible for the propagation of single dendrites (Figure 32).<sup>(23)</sup> The stability of dendritic web against dendritic breakdown is attributed to the fact that any interface protuberance is immediately eliminated by rapid layer spreading. The latent heat flow from the flat growth front further inhibits dendrite propagation. However, if the undercooling is too large, these nucleation barriers are overcome and random dendrite growth occurs.<sup>(21)</sup>

Several characteristics of our GaAs crystals impinge on the stability criteria for web growth. The overall faceting behavior of GaAs differed from Si in that web faces were composed of small, individual facets rather than one smooth ribbon face. This featured implies that 1) nucleation on the (111) faces was not as difficult in GaAs as in Si, and/or 2) steps and perturbations on the (111) GaAs ribbon faces were not removed by layer spreading. If these conditions apply to the interface facets as well as the ribbon faces, we would expect the GaAs interface to be less stable than the Si interface.

Also, Czochralski growth results<sup>(24)</sup> and our own dendrites illustrate subtle effects of the {111} polar planes on the faceting behavior of GaAs. Both Ga and As {111} faces are present on a faceted web interface, and evidence cited in Section V indicates that the polar nature of the compound may also contribute to destabilization of the interface. One is tempted to associate the polarity of the interface planes with the difficulty in growing three-twin-plane material, and with the predominance of the inverted interface in three-twin-plane crystals

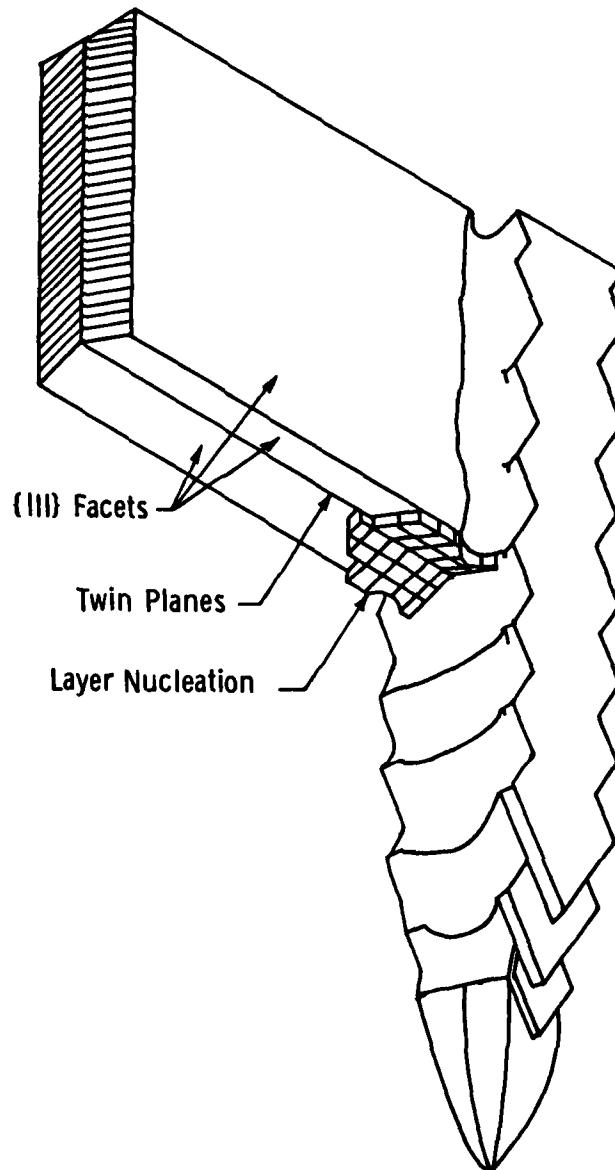


Figure 31 Schematic Section of Web Growth Illustrating the Faceted Interface. Layer Spreading is Initiated by Corner Nucleation at the Intersection of the Dendrite and the Web.

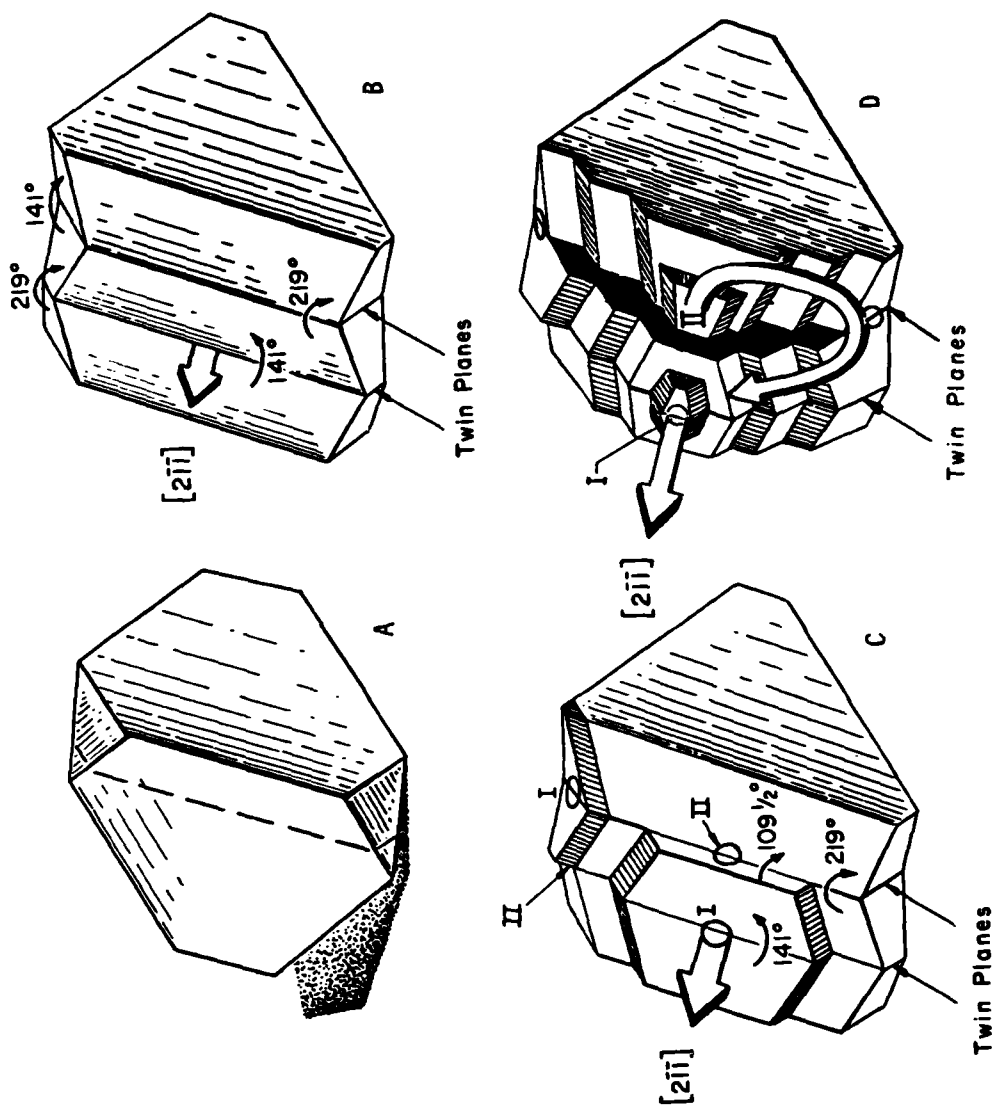


Figure 32 {111} Faceting in Untwinned and Twinned Diamond or Zinc Blende Solids. A) Equilibrium Form of the Untwinned Solid; B) Ridge and Reentrant Corner Structure Produced by Two Twin Planes; C&D) Nucleation at Type I Reentrant Corners Produces Type II Corners Generating an Indestructible System of Reentrancies By which Twinned Dendrites Propagate. (Adapted From Ref. 23).

and the Ga interface ( $[\bar{2}11]$  direction) in crystals where three-twin-planes degenerated into two.

The nucleation phenomena critical to web growth are dependent both on fundamental materials properties and on local thermal conditions. Therefore, macroscopic parameters that influence heat flow, such as undercooling, pull speed, seed thickness, and thermal geometry, also impact web stability. There is a "growth window" of suitable parameter ranges for which stable propagation of Si web will occur.

An analogous growth window may exist for GaAs and other polar compounds, but apparently it is greatly compressed due to characteristic attachment kinetics. Additional fundamental studies would be required to determine if the GaAs web "growth window" is realistically attainable.

## SECTION VII

### SUMMARY

We have developed a unique GaAs ribbon-growth system by applying dendritic web growth techniques to a liquid-encapsulated GaAs system. Computerized thermal modelling and experimental modification produced a thermal geometry from which 48 GaAs webs were grown. These crystals had a multidendrite and/or faceted morphology rather than typical web morphology. Crystal quality improved as thermal geometry, growth techniques, dendrite seeds, and melt chemistry were optimized during the course of the program; however, conventional web morphology was not achieved. Analyses of chemical modification, crystal-growth characteristics, and orientation relationships suggest that inherent materials properties of GaAs produce an atypical web morphology under conventional web-growth conditions.

Consequently, a simple transfer of Si web growth technology to our GaAs system was inadequate for the growth of high quality GaAs web. We believe that typical web morphology of GaAs and other polar compounds will be achieved only if sophisticated, fundamental studies determine specialized chemical and/or thermal conditions which will support conventional web growth of these materials.

#### REFERENCES

1. "Ribbon Growth of Single-Crystal GaAs for Solar Cell Application," Air Force Contract F33615-78-C-2031, Final Report No. AFAPL-TR-79-2094°, Westinghouse Electric Corporation (1979).
2. R. G. Seidensticker, et al., in Proc. 13th IEEE Photovoltaics Specialists Conf. (1978).
3. C. S. Duncan, et al., in Proc. 14th IEEE Photovoltaics Specialists Conf. (1980).
4. M. F. Amsterdam, et al., "Gallium Arsenide Dendrite Single-Crystal Program," Air Force Contract AF 33 (657)-8162, Final Report No. MLTDR 64-129, Westinghouse Electric Corporation (1964).
5. E. P. A. Metz, R. C. Miller, and R. Mazelsky, J. Appl. Phys. 33 (1962) 2016.
6. J. B. Mullin, B. W. Straughan, and W. S. Brickell, J. Phys. Chem. Solids 26 (1965) 782.
7. B. C. Grabmaier and J. G. Grabmaier, J. Crystal Growth 13 (1972) 635.
8. M. E. Weiner, D. T. Lassota, and B. Schwartz, J. Electrochem. Soc. 118 (1971) 301.
9. S. J. Bass and P. E. Oliver, in International Symposium on GaAs, 1966 (Institute of Physics and the Physical Society, London, 1966).
10. H. Lessoff and H. Swiggard, "Research on Gunn-Effect Materials (III-V Compounds)," NRL Memorandum Report 3360, Naval Research Laboratory (1976).
11. J. S. Haggerty and J. F. Wenckus, "Development of Techniques for the Growth of Bulk Single Crystals of Several III-V Compound Semiconductors," NASA Contract No. NAS 19-2020, Report No. N70-17301, Arthur D. Little, Inc. (1969).

REFERENCES (Cont.)

12. R. G. Seidensticker and R. H. Hopkins, J. Crystal Growth 50 (1980) 221.
13. J. W. Faust, in Compound Semiconductors, Volume 1: Preparation of III-V Compounds, Eds., R. K. Willardson and H. L. Goering (Reinhold, New York, 1962).
14. M. S. Abrahams and C. J. Buiochi, J. Appl. Phys. 36 (1965) 2855.
15. O. C. Ziekiewicz and Y. K. Chung, The Finite Element Method in Structural and Continuum Mechanics (McGraw-Hill, London, 1967), 228.
16. S. O'Hara and A. I. Bennett, J. Appl. Phys. 35 (1964) 686.
17. J. W. Faust and H. F. John, J. Electrochem. Soc. 180 (1961) 855.
18. O. Lindberg and J. W. Faust, in Compound Semiconductors, Volume 1: Preparation of III-V Compounds, Eds., R. K. Willardson and H. L. Goering (Reinhold, New York, 1962).
19. R. Moss and H. Nicholson, J. Electrochem. Soc. 107 (1960) 198C.
20. J. B. Mullin, in Crystal Growth and Characterization, Proc. of ISSCG2, Eds., R. Ueda and J. B. Mullin (North-Holland, Amsterdam, 1975).
21. R. G. Seidensticker, to be published.
22. J. F. Dewald, J. Electrochem. Soc. 104 (1957) 244.
23. D. R. Hamilton and R. G. Seidensticker, J. Appl. Phys. 31 (1960) 1165.
24. A. Steinemann and U. Zimmerli, Solid State Electronics 6 (1963) 597.

**DAT  
FILM**